NASA Contractor Report 168097

NUMERICAL SIMULATION OF AN ELECTROTHERMAL DEICER PAD

John J. Marano

The University of Toledo
Toledo, Ohio

March 1983

Prepared for

NATIONAL AERONAUTICS AND SPACE ADMINISTRATION
Lewis Research Center
Under Grant NAG 3-72

TABLE OF CONTENTS

NOMENCLATURE

$\hat{C}_p$	heat capacity	(Btu/lb-°F)
$C_1, \ldots, C_5$	constants in heater output function	
H	enthalpy	(Btu/ft^3)
h	heat transfer coefficient	(Btu/ft^2-hr-°F)
k	thermal conductivity	(Btu/ft-hr-°F)
L	latent heat of fusion for ice	(Btu/lb)
l	layer thickness	(ft)
Q	rate of heat production per unit volume	(Btu/hr-ft^3)
q	rate of heat production per unit area	(Btu/hr-ft^2 or Watts/in^2)
T	temperature	(°F)
t	time variable	(hr)
t_{on}, t_{off}	heater time on and time off	(hr)
U	dependent variable, H or T	
X	fraction of nodal volume which is ice	
x	space coordinate in one-dimension	(ft)
Y	fraction of nodal volume which is liquid water	
y	position of solid-liquid interface	(ft)

Greek letters:

α	thermal diffusivity	(ft^2/hr)
Δt	time step	(hr)
Δx	grid spacing	(ft)
ρ	density	(lb/ft^3)
ω	over-relaxation parameter	

Subscripts:

a1	inner ambient boundary
a2	outer ambient boundary
i	layer in composite blade
II	outer layer of composite blade (abrasion shield)
j	grid point
l	liquid (water)
lmp	liquid at the melting point
mp	melting point
s	solid (ice)
smp	solid at the melting point
w	ice-water layer

Superscripts:

'	point heat source
o	evaluated at the previous time level
Δ	evaluated halfway between the previous and present time level
(old)	value from previous iteration
(new)	value from current iteration

I. INTRODUCTION

The formation of ice on aircraft components poses a problem of considerable significance. For the aircraft to perform safely and efficiently at near or below freezing temperatures, this ice must be removed. Both anti-icing and de-icing systems are used for this purpose. An anti-icing system prevents the formation of ice, whereas a de-icing system periodically removes the ice that has formed. This investigation deals with electrothermal de-icing as applied to ice removal from propeller and helicopter rotor blades. As such, this is a continuation and extension of the work done by G. Baliga [1] at the University of Toledo.

A de-icer works by destroying the adhesion between the ice and the composite blade surface, thus allowing aerodynamic or centrifugal forces to sweep away the ice. This is accomplished in an electrothermal de-icer pad by means of a resistance heater which raises the temperature of the composite blade surface above the melting point of ice. Since only a thin layer of ice need be melted to destroy adhesion, the energy requirements are significantly less than those of other systems. Baliga [1] has reviewed the advantages and pitfalls of other anti-icing and de-icing systems.

A section of an electrothermal de-icer pad embedded in an aircraft blade is shown in Figure 1a. It is a composite

body consisting of five layers. The center layer is the heater, which is separated from the substrate and the abrasion shield by insulating layers. The bonding between these layers is suspected to be less than perfect, and small air pockets between layers may exist. In operation, the heater is turned on periodically to remove ice that has formed on the abrasion shield surface.

Typically, the heater is a woven mat of wires and glass fibers or multiple strips of resistance ribbon. Woven mats may have thicknesses as great as 0.020", whereas ribbons have thicknesses between 0.001" and 0.005". Individual heating elements are between 0.5" and 1.0" wide. Stallabrass [2] has pointed out that gaps which exist between these heating elements can reduce the effectiveness of the de-icer pad, causing non-uniform heating of the ice. The gap width is roughly 0.080" for woven mats and 0.040" for metal ribbons.

The two layers adjacent to the heater provide electrical insulation. In order to direct most of the heat outward, the outer layer should have a much higher thermal conductivity than the inner layer. This is generally not possible since good electrical insulators are also poor conductors of heat. To compensate for this effect, it is necessary to use a much greater thickness for the inner layer. A ratio of thicknesses of at least 2:1 has been recommended. Resin-impregnated cloth is commonly used for both layers. Electrical insulation requirements necessitate that the outer layer of cloth have a thickness between 0.010" and 0.020".

The purpose of the abrasion shield is to protect the de-icer from the environment and also to cut down drag on the composite blade surface. For these reasons, stainless steel is normally used for the abrasion shield. The relatively high thermal conductivity of stainless steel enables heat to be conducted laterally across the blade. This can be beneficial to melting the ice above the heater gaps. Thicknesses for the abrasion shield range from 0.010" to 0.020".

A wide range of materials is used as substrates depending on the particular application. An aluminum alloy is considered in this study. Baliga [1] and Stallabrass [2] have examined the effects of different materials and thicknesses on de-icer performance.

Due to the large number of parameters that affect the rate of heat transfer in the composite blade, it is not surprising that many proposed de-icer designs fail to achieve the level of performance expected. This complexity leads naturally to the use of numerical methods along with the digital computer to evaluate de-icer performance. In this study, de-icer performance is measured by the time required to melt the ice at the ice-abrasion shield interface (or a finite thickness of ice) starting from various initial temperatures. The model constructed considers one-dimensional, unsteady-state heat transfer in a composite body. A wide range of parameters are available to completely specify the de-icer design. The phase change in the ice

layer is accounted for by the Enthalpy method. This method and the numerical methods employed in the model are reviewed in the next section. The complete numerical formulation of the problem appears in Section III.

II. LITERATURE REVIEW

There have been several recent studies concerned with the performance of electrothermal de-icer pads. Of these, only the investigations of Baliga [1] and Stallabrass [2] have considered the effects of the phase change in the ice layer. Gent and Cansdale [3], while not considering the phase change in their simulation, do present temperature profiles from experimental de-icer pads. The de-icer pad model used in the present study takes into account the phase change, and also contains significant improvements over the models used in the studies mentioned above. All of these models have been one-dimensional except for that of Stallabrass, who also developed a two-dimensional model. The analytical and numerical methods used in the present and previous studies are outlined below.

A. ANALYTICAL METHODS

A variety of analytical techniques is available to solve transient heat conduction problems in composite bodies, the most common being the Laplace transformation. However, most of these techniques are too complicated to apply when the body contains more than two layers. An exception is a method proposed by Campbell [4], where the analogy between one-dimensional heat conduction and the flow of electricity along a transmission line is used to calculate

the temperature at any point within the composite body. Stallabrass [2] used Campbell's method to check the accuracy of his numerical technique. All analytical methods, however, have the disadvantage that an excessive amount of calculations must be done for each temperature desired. In addition, they cannot be used when the phase change in the ice layer is considered.

B. NUMERICAL METHODS

All of the recent models proposed for an electrothermal de-icer pad have used finite difference methods. In these methods, the differential equation governing the heat transfer in the composite body is replaced by a system of difference equations. This transforms the continuous time and space domain of the problem into a discrete grid of nodal points. The difference equations can then be solved algebraically to determine the temperature at all nodal points at any time step. This is a definite advantage over analytical methods. Finite differencing is an approximate technique, and its accuracy depends upon which of the several finite difference schemes is used along with the grid spacing (Δx and Δt) chosen. The accuracy is measured by the order of the truncation error for both the time and space derivatives. For some of these schemes, a restriction also exists on the size of Δx or Δt that will ensure convergence and stability of the solution. A finite difference representation of a de-icer pad appears in Figure 1b.

Both Stallabrass [2] and Gent and Cansdale [3] used the explicit forward finite difference scheme. In this scheme, the temperature at a node can be calculated directly from the nodal temperatures at the previous time step. The truncation error is first order in time and second order in space. The convergence and stability criteria for forward differencing is:

$\alpha\Delta t/(\Delta x)^2 \leq 1/2$ where α is the thermal diffusivity of the layer in the composite body. For the de-icer problem, this requires a time step of 0.001 sec. or smaller to be used. The excessive number of calculations needed because of this small time step can cause an accumulation of truncation and round-off error.

In Baliga's work [1] and in this study, the Crank-Nicolson implicit finite difference scheme is used. This method is unconditionally stable and no restrictions are placed on the size of Δt and Δx. In addition, the truncation error is second order for both time and space. This allows a time step of 0.1 sec. to be used, thus reducing the total number of calculations. The only drawback of this method is that the temperature at any grid point can no longer be explicitly calculated. The system of equations which results must be inverted or else solved iteratively in order to obtain the temperature distribution at any time step. Baliga used the method of Thomas to invert the tridiagonal system of equations. The method employed for the phase change in the present study dictates that Gauss-Seidel iteration be used.

This requires more calculations to be done but reduces round-off error.

C. METHODS FOR HANDLING THE PHASE CHANGE

In the past few years, there has been a significant increase in the number of articles appearing in the literature that deal with phase change and related moving boundary problems. These types of problems are sometimes referred to as Stefan problems. Due to the nonlinear boundary condition caused by the movement of the solid-liquid interface, these problems are relatively difficult to solve. Analytical solutions are only available for simple problems and many numerical techniques have been proposed. An extensive review of most of the analytical and numerical techniques that have been used appears in Reference 5. Many of these methods use predictor-corrector techniques, where the phase change interface location is assumed, and subsequent iterative calculations correct this position. This requires an excessive amount of calculation. The added complexity of the heat transfer occurring in the rest of the composite body makes these methods impractical for the de-icer problem. For this reason, methods which do not require trial and error calculations to determine the interface location have been used.

Stallabrass [2] accounted for the phase change by holding a node at the melting point until enough energy had been transferred to completely melt the nodal volume. Baliga [1] approximated the latent heat effect with a large change in heat capacity over a small temperature interval around the

melting point. The thermal conductivity was also allowed to vary linearly over the interval. This technique was proposed by Bonacina, et. al. [6]. Both methods are very similar to the Enthalpy method, but lack the formalism which makes this method easy to apply numerically. The Enthalpy method, which is also called the method of weak solution, is used in this investigation.

In the Enthalpy method, the governing equation for conservation of energy is formulated in terms of two dependent variables, enthalpy and temperature. The moving boundary condition and predictions of the phase change interface location are not needed. After the enthalpy at a node is calculated, the known enthalpy-temperature relationship for water can be used to determine the nodal temperature. The equivalence of this method to the moving boundary formulation was proven by Atthey [7].

Most of the applications of the Enthalpy method have been formulated using the forward finite difference scheme. In this study, the Crank-Nicolson scheme is used, and the system of equations which results is solved by Gauss-Seidel iteration. Voller and Cross [8,9] in two recent articles have pointed out that the Enthalpy method yields unrealistic results since a node remains at the melting point for a finite period of time. This leads to the prediction of temperatures which oscillate around their true values. The same phenomenon also occurs with the methods of Stallabrass and Baliga. By reinterpreting the Enthalpy method, Voller and Cross have derived a criterion for determining the points

of correspondence between the true and oscillating curves. This enables accurate temperature profiles to be obtained. The criterion is given in the "Discussion of Results" section.

III. NUMERICAL FORMULATION

A. GOVERNING EQUATIONS AND BOUNDARY CONDITIONS

The following assumptions were made in the formulation of a one-dimensional, unsteady-state, mathematical model for heat transfer in a composite aircraft blade on which an ice layer has formed:

1) The physical properties of the materials composing each layer of the composite blade are independent of temperature;
2) Lateral heat transfer in the layers can be neglected, so that only a one-dimensional model need be constructed;
3) The ambient temperature and all heat transfer coefficients are constant;
4) The ice layer thickness is constant;
5) The effect of the volume contraction of the ice as it melts can be neglected; and
6) The ice is "pure", so that the latent heat is released isothermally at the melting point.

1. Composite Aircraft Blade

With the above assumptions, the governing differential equation for each layer of the composite aircraft blade is:

$$\rho_i \hat{c}_{pi} \frac{\partial T_i}{\partial t} = k_i \frac{\partial^2 T_i}{\partial x^2} + Q_i \qquad i = 1, \ldots, II \qquad (1)$$

where T_i = temperature in layer i

Q_i = rate of heat production per unit volume in layer i

ρ_i = density of the ith layer

$\hat{c}_{pi}$ = heat capacity per unit mass of the ith layer

k_i = thermal conductivity of the ith layer

x = space coordinate

t = time variable

II = number of layers in the blade

A composite blade containing a finite thickness heater is characterized by:

i = 1 , substrate	$Q_1 = 0$
i = 2 , lower or inner insulation	$Q_2 = 0$
i = 3 , heater	$Q_3 = Q_3(t)$ (2)
i = 4 , upper or outer insulation	$Q_4 = 0$
i = II = 5, abrasion shield	$Q_5 = 0$

A variety of different boundary conditions is considered with equation (1). These are:

(i) For perfect contact between layers, the temperature and heat flux are continuous at the layer interfaces. This leads to the boundary conditions:

$$T_i\big|_I = T_{i+1}\big|_I \qquad (3a)$$

$$i=1,\ldots,II-1$$

$$-k_i \frac{\partial T_i}{\partial x}\bigg|_I = -k_{i+1} \frac{\partial T_{i+1}}{\partial x}\bigg|_I \qquad (3b)$$

where "I" denotes an interface.

(ii) In reality, there may exist a resistance to heat transfer across the layer interfaces due to the small layer of adhesive used to hold adjacent layers together and also to small air gaps caused by poor contact. The boundary conditions for this case are:

$$-k_i \frac{\partial T_i}{\partial x}\bigg|_I = h_i (T_i|_I - T_{i+1}|_I) = -k_{i+1} \frac{\partial T_{i+1}}{\partial x}\bigg|_I \qquad (4a,b)$$
$$i=1,\ldots,II-1$$

where h_i is the heat transfer coefficient across an interface.

(iii) If the heater can be treated as a point heat source (zero thickness), an alternate equation is used for the interfaces between layers, which is:

$$-k_i \frac{\partial T_i}{\partial x}\bigg|_I + q_i' = -k_{i+1} \frac{\partial T_{i+1}}{\partial x}\bigg|_I \quad i=1,\ldots,II-1 \qquad (5)$$

where q_i' is the rate of heat production per unit area. Equation (3a) still applies at an interface.

A blade with a point heat source is characterized by:

i = 1, substrate	$Q_1 = 0,\ q_1' = 0$
i = 2, inner insulation	$Q_2 = 0,\ q_2' = q_2'(t)$ (6)
i = 3, outer insulation	$Q_3 = 0,\ q_3' = 0$
i = II = 4, abrasion shield	$Q_4 = 0,\ q_4' = 0$

(iv) Convective heat transfer occurs at the inner boundary of the composite blade and also at the outer boundary if the ice layer is not present. For the inner boundary:

$$k_i \frac{\partial T_i}{\partial x}\bigg|_1 = h_{a1} (T_i|_1 - T_{a1}) \qquad i=1 \quad (7)$$

where "1" denotes the inner ambient boundary, h_{a1} is the convective heat transfer coefficient at the boundary and T_{a1} is the ambient temperature. Since the air within the blade is stagnant, h_{a1} is small.

(v) For the outer boundary:

$$-k_i \frac{\partial T_i}{\partial x}\bigg|_2 = h_{a2} \left(T_i\big|_2 - T_{a2}\right) \qquad i=II \qquad (8)$$

where "2" denotes the outer ambient boundary, h_{a2} is the convective heat transfer coefficient at the boundary and T_{a2} is the ambient temperature. The quantity h_{a2} is very large due to the dynamic forces acting on the outside of the blade.

Besides the above, constant temperature boundary conditions can be specified for the inner and outer surfaces of the composite blade. The initial temperature distribution in the composite blade can be constant or a function of position.

2. Heat Source

The total output of the heater is the same regardless of whether it is treated as being of finite or zero thickness. Thus, the total rate of heat production per unit area is:

$$q_i(t) = l_i Q_i(t) = q'_{i-1}(t) \qquad (9)$$

where l_i is the thickness of the heater. A wide range of different heater outputs can be specified. These include: outputs that are constant, linear or sinusoidal with time, and also outputs that can be periodically turned on and off: ramps, square waves, etc. The general expression for these functions is:

$$q_i(t) = \begin{cases} C_1 t + C_2 + C \cos (C_4 t + C_5), & 0 < t \leq t_{on} \\ 0, & t_{on} < t \leq P \end{cases}$$

$$P = t_{on} + t_{off}$$

$$q_i(t+P) = q_i(t), \quad t > P \tag{10}$$

where C_1, C_2, C_3, C_4 and C_5 are constants, t_{on} and t_{off} are the times the heater is on and off, respectively, and P is the period of the output.

3. Ice Layer

The classical formulation for the ice layer subject to assumptions (4), (5) and (6) is:

$$\rho_s \hat{C}_{ps} \frac{\partial T_s}{\partial t} = k_s \frac{\partial^2 T_s}{\partial x^2} \qquad x > y \tag{11a}$$

$$\rho_l \hat{C}_{pl} \frac{\partial T_l}{\partial t} = k_l \frac{\partial^2 T_l}{\partial x^2} \qquad x < y \tag{11b}$$

along with the moving boundary condition:

$$T_s = T_l = T_{mp} \qquad x = y \tag{12a}$$

$$k_s \left.\frac{\partial T_s}{\partial x}\right|_y - k_l \left.\frac{\partial T_l}{\partial x}\right|_y = \rho L \frac{d\dot{y}}{dt} \tag{12b}$$

where

T_s = temperature within the solid

T_l = temperature within the liquid

T_{mp} = melting point

ρ_s, $\hat{C}_{ps}$, k_s = physical properties of the solid

ρ_l, $\hat{C}_{p_l}$, k_l = physical properties of the liquid

ρL = latent heat of fusion per unit volume

$\dot{y}$ = position of the solid-liquid interface

As discussed in the "Literature Review", the solution of equations (11) and (12) requires that the interface location be solved for explicitly. To avoid this difficult procedure, the Enthalpy method is applied. The governing differential equation for the Enthalpy method is:

$$\frac{\partial H_w}{\partial t} = \frac{\partial}{\partial x}\left(k_w \frac{\partial T_w}{\partial x} \right) \tag{13}$$

where

H_w = enthalpy per unit volume within the ice-water layer

T_w = temperature within the ice-water layer

k_w = thermal conductivity within the ice-water layer

Thus, the enthalpy within both phases is found using only one equation. The known H_w vs. T_w relationship is used to determine T_w; this relationship is:

$$H_w = \begin{cases} \rho_s \hat{C}_{ps} T_w & , \ T_w < T_{mp} \\ \rho_l \hat{C}_{pl} (T_w - T_{mp}) + \rho_l (\hat{C}_{ps} T_{mp} + L) & , \ T_w > T_{mp} \end{cases} \tag{14}$$

where L is the latent heat of fusion per unit mass. It has been shown elsewhere [7] that the formulation above is equivalent to the moving boundary formulation, equations (11) and (12). For numerical solutions, it is easier to work with T_w as a function of H_w. Inversion of (14) gives:

$$T_w = \begin{cases} H_w/\rho_s \hat{c}_{ps} & , H_w \leq H_{smp} \\ T_{mp} & , H_{smp} < H_w < H_{lmp} \\ (H_w - H_{lmp})/\rho_l \hat{c}_{pl} + T_{mp} & , H \geq H_{lmp} \end{cases} \quad (15)$$

with

$$H_{smp} = \rho_s \hat{c}_{ps} T_{mp}$$

$$H_{lmp} = \rho_l (\hat{c}_{ps} T_{mp} + L)$$

where H_{smp} and H_{lmp} are the enthalpy of the solid and the liquid at the melting point, respectively. Also note that in equation (13), the thermal conductivity is now a function of position.

Boundary conditions must also be specified for the ice-water layer at the interfaces with the abrasion shield and the atmosphere. Perfect contact between the layer and the abrasion shield is assumed, so that equations (3a,b) apply with i+1=w, which are:

$$T_i\big|_I = T_w\big|_I \qquad i = II \quad (16a)$$

$$-k_i \frac{\partial T_i}{\partial x}\bigg|_I = -k_w \frac{\partial T_w}{\partial x}\bigg|_I \quad (16b)$$

Equation (8) holds for the outer boundary of the ice-water layer with i=w, which is:

$$-k_w \frac{\partial Tw}{\partial x}\bigg|_2 = h_{a2} \left(T_w\big|_2 - T_{a2}\right) \quad (17)$$

After a thin layer of ice has melted, the layer can be shed by the dynamic forces acting on the composite blade, and equation (8) applies at the outer boundary.

B. CRANK-NICOLSON FINITE DIFFERENCE FORMULATION

For numerical solutions, the above differential equations are replaced by their finite difference analogs. In this study, the Crank-Nicolson finite difference scheme is used.

Truncated series expansions are used in the Crank-Nicolson scheme to approximate the partial derivatives appearing in the governing equations. Letting U stand for the dependent variable, either T or H, truncated Taylor's series expansions for the partial derivatives $\frac{\partial U}{\partial x}$ and $\frac{\partial^2 U}{\partial x^2}$ are:

$$\left.\frac{\partial U}{\partial x}\right|_j = \frac{U_{j+1} - U_{j-1}}{2(\Delta x)} + O(\Delta x)^2 \qquad (18)$$

and

$$\left.\frac{\partial^2 U}{\partial x^2}\right|_j = \frac{U_{j+1} - 2U_j + U_{j-1}}{(\Delta x)^2} + O(\Delta x)^2 \qquad (19)$$

where the subscripts j-1, j and j+1 denote adjacent nodal values. The grid spacing, Δx, is constant within a layer, but may vary between different layers. Equation (13) requires the expansion for $\frac{\partial}{\partial x}\left(k \frac{\partial U}{\partial x}\right)$, which is:

$$\left.\frac{\partial}{\partial x}\left(k \frac{\partial U}{\partial x}\right)\right|_j = \frac{k_{j+1/2}(U_{j+1} - U_j) - k_{j-1/2}(U_j - U_{j-1})}{(\Delta x)^2} + O(\Delta x)^2 \qquad (20)$$

where $k_{j+1/2}$ and $k_{j-1/2}$ are average values of k between nodes j+1 and j, and nodes j and j-1, respectively. The truncation error for these approximations of the partial derivatives is second order. The second order finite difference analog for the time derivative, $\frac{\partial U}{\partial t}$, is:

$$\left.\frac{\partial U}{\partial t}\right|_j^{\Delta} = \frac{U_j - U_j^{\circ}}{\Delta t} + O(\Delta t)^2 \qquad (21)$$

where the superscript $^{\circ}$ denotes the value at the previous time level and the superscript $^{\Delta}$ denotes the value halfway between the previous and present time levels. The time step Δt can be changed as the calculations progress in time.

In the Crank-Nicolson scheme, the governing differential equations and boundary conditions are approximated at a point halfway between the known and unknown time levels. The approximation for the time derivative is given by equation (21). The analogs for the space derivatives given in equations (18, 19 and 20), however, cannot be used since they would require the evaluation of the dependent variable at the half time level. To overcome this difficultly, the Crank-Nicolson scheme employs the following approximations for these derivatives:

$$\left.\frac{\partial U}{\partial x}\right|_j^{\Delta} = \frac{1}{2}\left(\left.\frac{\partial U}{\partial x}\right|_j + \left.\frac{\partial U}{\partial x}\right|_j^{\circ}\right)$$

$$= \frac{U_{j+1} - U_{j-1} + U_{j+1}^{\circ} - U_{j-1}^{\circ}}{4\Delta x} + O(\Delta x)^2 \qquad (22)$$

$$\left.\frac{\partial^2 U}{\partial x^2}\right|_j^{\Delta} = \frac{1}{2}\left(\left.\frac{\partial^2 U}{\partial x^2}\right|_j + \left.\frac{\partial^2 U}{\partial x^2}\right|_j^{\circ}\right)$$

$$= \frac{U_{j+1} - 2U_j + U_{j-1} + U_{j+1}^{\circ} - 2U_j^{\circ} + U_{j-1}^{\circ}}{2(\Delta x)^2} + O(\Delta x)^2 \qquad (23)$$

$$\frac{\partial}{\partial x}\left(k\frac{\partial U}{\partial x}\right)\Big|_j^{\Delta} = \frac{1}{2}\left[\frac{\partial}{\partial x}\left(k\frac{\partial U}{\partial x}\right)\Big|_j + \frac{\partial}{\partial x}\left(k\frac{\partial U}{\partial x}\right)\Big|_j^{o}\right] \tag{24}$$

$$= \frac{k_{j+1/2}(U_{j+1}-U_j) - k_{i-1/2}(U_j-U_{j-1}) + k^o_{j+1/2}(U^o_{j+1}-U^o_j) - k^o_{j-1/2}(U^o_j - U^o_{j-1})}{2(\Delta x)^2}$$

$$+ O(\Delta x)^2$$

In addition, the approximation for U_j evaluated at the half time level is:

$$U_j^{\Delta} = \frac{1}{2}\ (U_j + U_j^o) + O(\Delta t)^2 \tag{25}$$

The Crank-Nicolson finite difference equations are obtained by substituting the above into the governing differential equations and boundary conditions of Part A.

C. FINITE DIFFERENCE EQUATIONS FOR THE COMPOSITE AIRCRAFT BLADE

Substitution of the analogs (21) and (23) into equation (1) yields:

$$\rho_i \hat{c}_{pi}\ \frac{T_{i,j} - T^o_{i,j}}{\Delta t} =$$

$$k_i\ \frac{T_{i,j+1} - 2\,T_{i,j} + T_{i,j-1} + T^o_{i,j+1} - 2\,T^o_{i,j} + T^o_{i,j-1}}{2(\Delta x_i)^2} \tag{26a}$$

$$+ Q_i \qquad\qquad i=1,\ldots,II$$

Solving for the unknown temperature at node j gives:

$$T_{i,j} = \left(T_{i,j+1} + T_{i,j-1} + T^o_{i,j+1} + 2(M_i-1)\ T^o_{i,j} + T^o_{i,j-1} + 2S_i\right) \Big/ 2(M_i+1) \tag{26b}$$

where $M_i = (\Delta x_i)^2/\alpha_i \Delta t$

$S_i = Q_i(\Delta x_i)^2/k_i$

$\alpha_i = k_i/\rho_i \hat{c}_{pi}$

The quantity α_i is the thermal diffusivity of the ith layer. The source term, S_i, is a function of time and so is evaluated at the half time step. Equation (26) is valid for all grid points within each of the layers, 1 through II. An alternate expression is developed later for the ice layer. At the interfaces between layers and at the inner and outer surfaces of the composite blade, the boundary conditions must be finite differenced. The finite difference analogs of conditions (i) through (v) of Part A are given below:

1. Perfect Contact Interface - B.C. (i)

For this case, let j be the interfacial node between the layers i and i+1 as shown in Figure 2a. Finite differencing equation (3) with the aid of analog (22) gives:

$$T_{i,j} = T_{i+1,j} \quad , \quad T^{\circ}_{i,j} = T^{\circ}_{i+1,j} \qquad i=1,\ldots,II-1 \tag{27a}$$

and

$$-k_i \frac{T_{i,j+1} - T_{i,j-1} + T^{\circ}_{i,j+1} - T^{\circ}_{i,j-1}}{4\Delta x_i} =$$

$$-k_{i+1} \frac{T_{i+1,j+1} - T_{i+1,j-1} + T^{\circ}_{i+1,j+1} - T^{\circ}_{i+1,j-1}}{4\Delta x_{i+1}} \tag{27b}$$

The nodal temperatures $T_{i,j+1}$, $T^{o}_{i,j+1}$, $T_{i+1,j-1}$ and $T^{o}_{i+1,j-1}$ are fictitious values and must be eliminated from the finite difference expression. This is done by the application of equation (26) to node j for both layers i and i+1. This yields:

$$T_{i,j+1} + T^{o}_{i,j+1} =$$

$$2(M_i+1)\ T_{i,j} - T_{i,j-1} - 2(M_i-1)\ T^{o}_{i,j} - T^{o}_{i,j-1} - 2S_i \qquad (28a)$$

$$T_{i+1,j-1} + T^{o}_{i+1,j-1} =$$

$$2(M_{i+1}+1)T_{i+1,j} - T_{i+1,j+1} - 2(M_{i+1}-1)T^{o}_{i+1,j} - T^{o}_{i+1,j+1} - 2S_{i+1} \qquad (28b)$$

Equations (27a,b) and (28a,b) can be combined to eliminate the fictious temperatures, yielding:

$$T_{i,j} = \Big(T_{i,j-1} + N_i\ T_{i+1,j+1} + T^{o}_{i,j-1} + [(M_i-1) + N_i(M_{i+1}-1)]\ T^{o}_{i,j} + N_i\ T^{o}_{i+1,j+1} + S_i + N_i S_{i+1}\Big) \Big/ [(1+M_i) + N_i(1+M_{i+1})] \qquad (29)$$

$$i=1,\ldots,II-1$$

where $N_i = k_{i+1}\Delta x_i / k_i \Delta x_{i+1}$

2. Resistive Interface - B.C. (ii)

Let j be the interfacial node for layer i and j+1 be the interfacial node for layer i+1. This is shown in Figure 2b. Substituting the analogs (22) and (25) into equation (4a) gives:

$$-k_i \frac{T_{i,j+1} - T_{i,j-1} + T^o_{i,j+1} - T^o_{i,j-1}}{4\Delta x_i} =$$

$$h_i\left(\frac{1}{2}(T_{i,j} + T^o_{i,j}) - \frac{1}{2}(T_{i+1,j+1} + T^o_{i+1,j+1})\right) \qquad (30)$$

$$i=1,\ldots,II-1$$

Using equation (28a), the fictitious temperatures $T_{i,j+1}$ and $T^o_{i,j+1}$ can be eliminated. Thus, the equation for $T_{i,j}$ at this interface is, after rearrangement:

$$T_{i,j} = \left(T_{i,j-1} + R_{1i}\, T_{i+1,j+1} + T^o_{i,j-1} - (1-M_i + R_{1i})\, T^o_{i,j} + R_{1i}\, T^o_{i+1,j+1} + S_i\right)\Big/(1 + M_i + R_{1i}) \qquad (31)$$

where

$$R_{1i} = \frac{\Delta x_i h_i}{k_i}$$

Similarly, for boundary condition (4b):

$$-k_{i+1} \frac{T_{i+1,j+2} - T_{i+1,j} + T^o_{i+1,j+2} - T^o_{i+1,j}}{4\Delta x_{i+1}} =$$

$$h_i\left(\frac{1}{2}(T_{i,j} + T^o_{i,j}) - \frac{1}{2}(T_{i+1,j+1} + T^o_{i+1,j+1})\right) \qquad (32)$$

$$i=1,\ldots,II-1$$

Equation (28b) written for layer i+1 is used to eliminate $T_{i+1,j}$ and $T^o_{i+1,j}$. This yields:

$$T_{i+1,j+1} = \left(T_{i+1,j+2} + R_{2i}T_{i,j} + T^o_{i+1,j+2} - (1-M_{i+1}+R_{2i})\cdot T^o_{i+1,j+1} + R_{2i}T^o_{i,j} + S_{i+1}\right)\Big/(1+M_{i+1}+R_{2i}) \qquad (33)$$

where $R_{2i} = \dfrac{\Delta x_{i+1} h_i}{k_{i+1}}$

3. Point Heat Source - B.C. (iii)

The same grid as used for (i) (Figure 2a) is used for this interface. Applying the Crank-Nicolson derivative approximations, the finite difference analog of equation (5) is:

$$-k_i \frac{T_{i,j+1} - T_{i,j-1} + T^o_{i,j+1} - T^o_{i,j-1}}{4\Delta x_i} + q'_i =$$

(34)

$$-k_{i+1} \frac{T_{i+1,j+1} - T_{i+1,j-1} + T^o_{i+1,j+1} - T^o_{i+1,j-1}}{4\Delta x_{i+1}}$$

$i=1,\ldots,II-1$

Equations (28a,b) with $S_i=S_{i+1}=0$ and $T_{i,j} = T_{i+1,j}$ and $T^o_{i,j} = T^o_{i+1,j}$ are used to eliminate the fictitious temperatures $T_{i,j+1}$, $T^o_{i,j+1}$, $T_{i+1,j-1}$ and $T^o_{i+1,j-1}$. The finite difference expression for $T_{i,j}$ at the interface is:

$$T_{i,j} = \Big(T_{i,j-1} + N_i T_{i+1,j+1} + T^o_{i,j-1} + [(M_i-1) + N_i(M_{i+1}-1)]\, T^o_{i,j} + N_i\, T^o_{i+1,j+1} + 2\, S'_i\Big) \Big/ [(1+M_i) + N_i\,(1+M_{i+1})] \qquad (35)$$

where $S'_i = q'_i\, \Delta x_i / k_i$

Like S_i, S_i' is evaluated at the half time step. The similarity of this equation and equation (29) allows them to be combined for computer implementation.

4. Inner Ambient Interface - B.C. (iv)

The grid used for the boundary between the substrate and the interior of the composite blade is shown in Figure 2c. At this surface i=1, j=1. The finite difference form for equation (7) is:

$$k_1 \frac{T_{1,2} - T_{1,0} + T^{\circ}_{1,2} - T^{\circ}_{1,0}}{4\Delta x_1} = h_{a1}\left(\frac{1}{2}(T_{1,1} + T^{\circ}_{1,1}) - T_{a1}\right) \quad (36)$$

Temperatures $T_{1,0}$ and $T^{\circ}_{1,0}$ are fictitious and are eliminated by the same procedure as used for the other boundary conditions, this gives for $T_{1,1}$:

$$T_{1,1} = \left(T_{1,2} - (1-M_1 + N_{a1})\, T^{\circ}_{1,1} + T^{\circ}_{1,2} + 2\, N_{a1} T_{a1}\right) \quad (37)$$
$$/(1 + M_1 + N_{a1})$$

where $N_{a1} = \Delta x_1 h_{a1}/k_1$

5. Outer Ambient Interface - B.C. (v)

When the ice layer is not present, the grid at the outer surface of the abrasion shield is that shown in Figure 2d. At this surface i=II, and let j be the interfacial node. Finite differencing equation (8) yields:

$$-k_{II}\frac{T_{II,j+1} - T_{II,j-1} + T^{o}_{II,j+1} - T^{o}_{II,j-1}}{4\Delta x_{II}} = h_{a2}\left(\frac{1}{2}(T_{II,j} + T^{o}_{II,j}) - T_{a2}\right) \tag{38}$$

The fictitious temperatures, $T_{II,j+1}$ and $T^{o}_{II,j+1}$, are eliminated as previously described to give:

$$T_{II,j} = \left(T_{II,j-1} - (1 - M_{II} + N_{a2})\, T^{o}_{II,j} + T^{o}_{II,j-1} + 2\, N_{a2}\, T_{a2}\right) \Big/ (1 + M_{II} + N_{a2}) \tag{39}$$

where $N_{a2} = \Delta x_{II} h_{a2} / k_{II}$

D. FINITE DIFFERENCE EQUATIONS FOR THE ICE LAYER

Unlike the composite blade, two equations are needed at each node of the ice layer; one to calculate enthalpy and one to calculate temperature. Substitution of analogs (21) and (24) into equation (13) yields the difference equation to be used in the Enthalpy method:

$$\frac{H_{w,j} - H^{o}_{w,j}}{\Delta t} = \Big(k_{w,j+1/2}(T_{w,j+1} - T_{w,j}) - k_{w,j-1/2}(T_{w,j} - T_{w,j-1}) + k^{o}_{w,j+1/2}(T^{o}_{w,j+1} - T^{o}_{w,j}) - k^{o}_{w,j-1/2}(T^{o}_{w,j} - T^{o}_{w,j-1})\Big) \Big/ 2(\Delta x_{w})^{2} \tag{40}$$

The equation above must be solved explicitly for the nodal enthalpy, $H_{w,j}$. This requires equation (15) to be used to relate $T_{w,j}$ to $H_{w,j}$. Note that this leads to three sets of equations; one each for the node below, at, and above the

melting point. Substitution of (15) and rearrangement yields, for the solid range:

$$H_{w,j} = \Big(H^{\circ}_{w,j} + M_w/2\,[k_{w,j+1/2}T_{w,j+1} + k_{w,j-1/2}T_{w,j-1} + k^{\circ}_{w,j+1/2}\cdot (T^{\circ}_{w,j+1} - T^{\circ}_{w,j}) - k^{\circ}_{w,j-1/2}(T^{\circ}_{w,j} - T^{\circ}_{w,j-1})]\Big) \Big/ [1 + \tfrac{1}{2}(M_w/\rho_s \hat{C}_{ps})\ (k_{w,j+1/2} + k_{w,j-1/2})] \qquad (41a)$$

$$H_{w,j} \leq H_{smp}$$

with $$T_{w,j} = H_{w,j}/\rho_s \hat{C}_{ps} \qquad (41b)$$

for the melting range:

$$H_{w,j} = H^{\circ}_{w,j} + M_w/2\,[k_{w,j+1/2}(T_{w,j+1} - T_{mp}) - k_{w,j-1/2}\cdot (T_{mp} - T_{w,j-1}) + k^{\circ}_{w,j+1/2}(T^{\circ}_{w,j+1} - T^{\circ}_{w,j}) - k^{\circ}_{w,j-1/2}(T^{\circ}_{w,j} - T^{\circ}_{w,j-1})] \qquad (42a)$$

$$H_{smp} < H_{w,j} < H_{lmp}$$

with $$T_{w,j} = T_{mp} \qquad (42b)$$

and for the liquid range:

$$H_{w,j} = \Big(H^{\circ}_{w,j} + M_w/2\,[k_{w,j+1/2}(T_{w,j+1} - T_{mp} + H_{lmp}/\rho_l \hat{C}_{pl}) - k_{w,j-1/2}(T_{mp} - H_{lmp}/\rho_l \hat{C}_{pl} - T_{w,j-1}) + k^{\circ}_{w,j+1/2}(T^{\circ}_{w,j+1} - T^{\circ}_{w,j}) - k^{\circ}_{w,j-1/2}(T^{\circ}_{w,j} - T^{\circ}_{w,j-1})]\Big) \Big/ [1 + \tfrac{1}{2}(M_w/\rho_l \hat{C}_{pl})(k_{w,j+1/2} + k_{w,j-1/2})] \qquad (43a)$$

$$H_{w,j} \geq H_{lmp}$$

with $$T_{w,j} = (H_{w,j} - H_{lmp})/\rho_l \hat{c}_{pl} + T_{mp} \qquad (43b)$$

where $$M_w = \Delta t/(\Delta x_w)^2$$

The algorithm used to implement these equations is presented later. When node j is solid at both the present and previous time levels, equations (41a,b) can be combined. The resulting equation for $T_{w,j}$ is equivalent to equation (26b). This equivalence also holds when node j is liquid at both time levels and (43a,b) are combined.

Equation (42) has a different form from (41) and (43). The node is held at the melting point, and heat entering the nodal volume is used only for melting. Thus, the fraction of the nodal volume melted can be related to the enthalphy of the node calculated using (42a). Letting X_j be the fraction of the node which is solid and Y_j be the fraction of the node which is liquid, an energy balance yields:

$$H_{w,j} = H_{smp} X_j + H_{lmp} Y_j \qquad (44)$$

where X_j and Y_j are related by: $X_j + Y_j = 1$. The movement of the ice-water interface through the layer can be followed by using equation (44).

Equation (42) can also be derived by finite differencing the moving boundary condition (12) and applying (44). Equation (12) is applied to a single node, and then finite differenced to give:

$$T_{w,j} = T_{mp} \qquad (45a)$$

$$k_w \left.\frac{\partial T_w}{\partial x}\right|_{j+}^{\Delta} - k_w \left.\frac{\partial T_w}{\partial x}\right|_{j-}^{\Delta} = \rho L \left.\frac{dy}{dt}\right|_{j}^{\Delta} \qquad (45b)$$

The approximations for the first derivatives with respect to x used in (45b) are slightly different than equation (22). They are:

$$k_w \left.\frac{\partial T_w}{\partial x}\right|_{j-}^{\Delta} =$$

$$\frac{k_{w,j-1/2}(T_{w,j} - T_{w,j-1}) + k^{o}_{w,j-1/2}(T^{o}_{w,j} - T^{o}_{w,j-1})}{2\Delta x_w} \qquad (46a)$$

$$k_w \left.\frac{\partial T_w}{\partial x}\right|_{j+}^{\Delta} =$$

$$\frac{k_{w,j+1/2}(T_{w,j+1} - T_{w,j}) + k^{o}_{w,j+1/2}(T^{o}_{w,j+1} - T^{o}_{w,j})}{2\Delta x_w} \qquad (46b)$$

The latent heat of melting per unit volume, ρL, is (neglecting volume contraction) equal to $(H_{lmp} - H_{smp})$. Using analog (21) for the time derivative and substituting the above finite difference analogs into equation (45b) yields:

$$(H_{lmp} - H_{smp})\frac{y_j - y_j^{o}}{\Delta t} = \frac{k_{w,j+1/2}(T_{w,j+1} - T_{mp}) + k^{o}_{w,j+1/2}(T^{o}_{w,j+1} - T^{o}_{w,j}) - k_{w,j-1/2}(T_{mp} - T_{w,j-1}) - k^{o}_{w,j-1/2}(T^{o}_{w,j} - T^{o}_{w,j-1})}{2\Delta x_w} \qquad (47)$$

Dividing equation (47) by Δx_w, the left hand side of the equation becomes:

$$(H_{lmp} - H_{smp}) \frac{Y_j/\Delta x_w - Y_j^o/\Delta x_w}{\Delta t} = (H_{lmp} - H_{smp}) \frac{Y_j - Y_j^o}{\Delta t}$$

$$= \frac{H_{lmp}Y_j - H_{smp}(1 - X_j) - H_{lmp}Y_j^o + H_{smp}(1 - X_j^o)}{\Delta t} \quad (48)$$

$$= \frac{(H_{smp}X_j + H_{lmp}Y_j) - H_{smp} + H_{smp} - (H_{smp}X_j^o + H_{lmp}Y_j^o)}{\Delta t}$$

$$= \frac{H_{w,j} - H_{w,j}^o}{\Delta t}$$

In the above, equation (44) was used along with the fact that $Y_j = \frac{Y_j}{\Delta x_w}$. Substitution into equation (47) yields:

$$\frac{H_{w,j} - H_{w,j}^o}{\Delta t} = \frac{k_{w,j+1/2}(T_{w,j+1} - T_{mp}) - k_{w,j-1/2}(T_{mp} - T_{w,j-1})}{2\ (\Delta x_w)^2}$$

$$+ \frac{k_{w,j+1/2}^o(T_{w,j+1}^o - T_{w,j}^o) - k_{w,j-1/2}^o(T_{w,j}^o - T_{w,j-1}^o)}{}$$

or

$$H_{w,j} = H_{w,j}^o + M_w/2\,[k_{w,j+1/2}(T_{w,j+1} - T_{mp}) - k_{w,j-1/2} \cdot (T_{mp} - T_{w,j-1}) + k_{w,j+1/2}^o(T_{w,j+1}^o - T_{w,j}^o) - k_{w,j-1/2}^o(T_{w,j}^o - T_{w,j-1}^o)]$$

The final result is equation (42a). From the above analysis, it is apparent that the Enthalpy method is a much easier and more direct method to derive the melting point equation. This analysis, however, does show the equivalence of the classical and Enthalpy method formulations.

As noted earlier, in the Enthalpy method formulation, k_w is a function of position. More specifically, it is a function of the liquid-solid interface position. Equations (41) through (43) require average values for k_w between adjacent nodes. A volume average is used to ensure that the correct values are obtained when $X_j = \frac{1}{2}$. The quantity $k_{w,j-1/2}$ is the volume average thermal conductivity between nodes j-1 and j, and $k_{w,j+1/2}$ is the volume average thermal conductivity between nodes j and j+1. Figure 3a through d show the averages used for different interface locations. When $X_j = \frac{1}{2}$, $k_{w,j-1/2} = k_l$ and $k_{w,j+1/2} = k_s$, which are the correct values to be used when the interface lies exactly on node j. It should also be noted that due to the method used to average k_w, the computer algorithm is, in general, only valid when the solid region is above the liquid region.

Equations (41) through (43) are not used at the abrasion shield-ice interface or at the outer surface of the layer. At these surfaces, the boundary conditions (16) and (17) are finite differenced. The differencing procedure is essentially the same as that used for the boundary conditions previously encountered. The finite difference equations used at these surfaces are given below:

1. Abrasion Shield - Ice Interface

The grid shown in Figure 2a with i=II and i+1=w is used at this interface. Due to the dependence of k_w on position, an alternate finite difference analog for $k_w \frac{\partial T_w}{\partial x}$ is used in equation (16b). The analog is obtained by taking the average of equations (46a,b); that is:

$$k_w \frac{\partial T_w}{\partial x}\bigg|^{\Delta}_{j} = \frac{1}{2}\left(k_w \frac{\partial T_w}{\partial x}\bigg|^{\Delta}_{j+} + k_w \frac{\partial T_w}{\partial x}\bigg|^{\Delta}_{j-}\right) \tag{49}$$

Then, substituting the above and analog (22) into boundary condition (16b) and finite differencing (16a) yields:

$$T_{II,j} = T_{w,j} \quad , \quad T^{o}_{II,j} = T^{o}_{w,j} \tag{50a}$$

$$-k_{II}\frac{T_{II,j+1} - T_{II,j-1} + T^{o}_{II,j+1} - T^{o}_{II,j-1}}{4\Delta x_{II}} = \tag{50b}$$

$$-\frac{k_{w,j+1/2}(T_{w,j+1} - T_{w,j}) + k_{w,j-1/2}(T_{w,j} - T_{w,j-1}) +}{4\Delta x_{w}} \cdots$$

$$\underline{k^{o}_{w,j+1/2}(T^{o}_{w,j+1} - T^{o}_{w,j}) + k^{o}_{w,j-1/2}(T^{o}_{w,j} - T^{o}_{w,j-1})}$$

Equation (26) with i=II is used to eliminate the fictitious temperatures $T_{II,j+1}$ and $T^{o}_{II,j+1}$, and equation (40) is used to eliminate the fictitious quantities $k_{w,j-1/2}(T_{w,j} - T_{w,j-1})$ and $k^{o}_{w,j-1/2}(T^{o}_{w,j} - T^{o}_{w,j-1})$ in (50b). Combination of the resulting equation with equation (50a) and (15) yields,

for the solid range:

$$H_{w,j} = \Big(H^{\circ}_{w,j} + M_w N_w [T_{II,j-1} + T^{\circ}_{II,j-1} + (M_{II} - 1) \cdot T^{\circ}_{w,j}] + M_w [k_{w,j+1/2} T_{w,j+1} + k^{\circ}_{w,j+1/2} (T^{\circ}_{w,j+1} - T^{\circ}_{w,j})] \Big) \Big/ [1 + (M_w / \rho_s \hat{c}_{ps})(k_{w,j+1/2} + N_w + M_{II} N_w)] \tag{51a}$$

$$H_{w,j} \leq H_{smp}$$

with $$T_{w,j} = H_{w,j} / \rho_s \hat{c}_{ps} \tag{51b}$$

for the melting range:

$$H_{w,j} = H^{\circ}_{w,j} + M_w N_w [T_{II,j-1} - (M_{II} + 1)\, T_{mp} + T^{\circ}_{II,j-1} + (M_{II} - 1)\, T^{\circ}_{w,j}] + M_w [k_{w,j+1/2} (T_{w,j+1} - T_{mp}) + k^{\circ}_{w,j+1/2} (T^{\circ}_{w,j+1} - T^{\circ}_{w,j})] \tag{52a}$$

$$H_{smp} < H_{w,j} < H_{lmp}$$

with $$T_{w,j} = T_{mp} \tag{52b}$$

for the liquid range:

$$H_{w,j} = \Big(H^{\circ}_{w,j} + M_w N_w [T_{II,j-1} - (M_{II} + 1)(T_{mp} - H_{lmp} / \rho_l \hat{c}_{pl}) + T^{\circ}_{II,j-1} + (M_{II} - 1) T^{\circ}_{w,j}] + M_w [k_{w,j+1/2} (T_{w,j+1} - T_{mp} + H_{lmp} / \rho_l \hat{c}_{pl}) + k^{\circ}_{w,j+1/2} (T^{\circ}_{w,j+1} - T^{\circ}_{w,j})] \Big) \Big/ [1 + \tag{53a}$$

$$(M_w/\rho_l \hat{C}_{pl})(k_{w,j+1/2} + N_w + M_{II}N_w)] \qquad \text{(53a) continued}$$

$$H_{w,j} \geq H_{lmp}$$

with $$T_{w,j} = (H_{w,j} - H_{lmp})/\rho_l \hat{C}_{pl} + T_{mp} \qquad \text{(53b)}$$

where $$N_w = k_{II}\Delta x_w/\Delta x_{II}$$

When node j is either solid or liquid, equation (51) or (53) reduces to equation (29).

2. Ice-Ambient Interface

The grid shown in Figure 2d with II=w applies at this interface. Substituting the finite difference analogs (25) and (49) into boundary condition (17) gives:

$$- \frac{k_{w,j+1/2}(T_{w,j+1} - T_{w,j}) + k_{w,j-1/2}(T_{w,j} - T_{w,j-1})}{4\Delta x_w} + \cdots$$

$$\frac{k^o_{w,j+1/2}(T^o_{w,j+1} - T^o_{w,j}) + k^o_{w,j-1/2}(T^o_{w,j} - T^o_{w,j-1})}{} = \qquad \text{(54)}$$

$$h_{a2}\left(\frac{1}{2}(T_{w,j} + T^o_{w,j}) - T_{a2}\right)$$

The quantities $k_{w,j+1/2}(T_{w,j+1} - T_{w,j})$ and $k^o_{w,j+1/2}(T^o_{w,j+1} - T^o_{w,j})$ are eliminated using equation (40), and combination of the result with (15) yields, for the solid range:

$$H_{w,j} = \left(H^o_{w,j} + M_w N_{a2,w}[2T_{a2} - T^o_{w,j}] + M_w \cdot \right. \qquad \text{(55a)}$$

$$\left.[k_{w,j-1/2}T_{w,j-1} + k^o_{w,j-1/2}(T^o_{w,j-1} - T^o_{w,j})]\right)/$$

$$[\,1 + (M_w/\rho_s \hat{C}_{ps})(k_{w,j-1/2} + N_{a2,w})\,] \qquad \text{(55a) continued}$$

$$H_{w,j} \leq H_{smp}$$

with $$T_{w,j} = H_{w,j}/\rho_s \hat{C}_{ps} \qquad \text{(55b)}$$

for the melting range:

$$H_{w,j} = H^{\circ}_{w,j} + M_w N_{a2,w} [\,2\,T_{a2} - T_{mp} - T^{\circ}_{w,j}] + \qquad \text{(56a)}$$

$$M_w [k_{w,j-1/2}(T_{w,j-1} - T_{mp}) + k^{\circ}_{w,j-1/2}(T^{\circ}_{w,j-1} - T^{\circ}_{w,j})]$$

$$H_{smp} < H_{w,j} < H_{lmp}$$

with $$T_{w,j} = T_{mp} \qquad \text{(56b)}$$

for the liquid range:

$$H_{w,j} = \Big(H^{\circ}_{w,j} + M_w N_{a2,w} [\,2\,T_{a2} - T_{mp} + H_{lmp}/ \qquad \text{(57a)}$$

$$\rho_l \hat{C}_{pl} - T^{\circ}_{w,j}] + M_w [k_{w,j-1/2}(T_{w,j-1} - T_{mp} + H_{lmp}/\rho_l \hat{C}_{pl}) +$$

$$k^{\circ}_{w,j-1/2}(T^{\circ}_{w,j-1} - T^{\circ}_{w,j})]\Big) \Big/ [\,1 + (M_w/\rho_l \hat{C}_{pl})(k_{w,j-1/2} + N_{a2,w})\,]$$

$$H_{w,j} \geq H_{lmp}$$

with $$T_{w,j} = (H_{w,j} - H_{lmp})/\rho_l \hat{C}_{pl} + T_{mp} \qquad \text{(57b)}$$

where $$N_{a2,w} = h_{a2} \Delta x_w$$

Just like the other solid and liquid equations, (55) and (57) can be reduced to give equation (39).

IV. COMPUTER IMPLEMENTATION

A. METHOD OF SOLUTION

The Crank-Nicolson finite differencing procedure results in a tridiagonal set of linear equations that must be solved at each time level. Each equation relates the unknown temperatures $T_{i,j-1}$, $T_{i,j}$ and $T_{i,j+1}$ at the current time level. The system of equations is solved by iteration because the phase of a node in the ice-water layer must be determined as the calculations proceed. The use of matrix inversion methods would require the phase of a node to be known prior to the beginning of the calculations. The Gauss-Seidel method was chosen as the iteration procedure because of its desirable convergence properties.

The Gauss-Seidel method requires initial estimates of the value of the dependent variable at each node. These are obtained by either assigning the values calculated at the previous time step or by using linear extrapolation from the past to the present time level. Linear extrapolated values tend to speed up the convergence of the iteration. A series of passes is made through the grid, $j=1,2,\ldots$, in which the value of the dependent variable is calculated at each node. This process is terminated when some convergence criterion is met. In these sweeps through the grid, the most current values are always used in the

calculations. For example, equation (26b) can be rewritten as:

$$T_{i,j}^{(new)} = \left(T_{i,j+1}^{(old)} + T_{i,j-1}^{(new)} + T_{i,j+1}^{o} + 2\,(M_i - 1)\cdot T_{i,j}^{o} + T_{i,j-1}^{o} + 2\,S_i\right) / 2\,(M_i + 1) \tag{58}$$

where $T_{i,j+1}^{(old)}$ is a value from the previous iteration and $T_{i,j-1}^{(new)}$ is a new value computed prior to computing $T_{i,j}^{(new)}$

All of the other finite difference equations can be rewritten in the same form as (58). The convergence criterion used is that the difference between two successive pass values must be less than some specified small value at each node. In most cases, 0.005% was used.

To accelerate convergence, which typically was slow, over-relaxation methods were used. These methods could not be applied to the ice-water layer equations due to stability problems, and were only used for the composite blade. The successive over-relaxation (SOR) method yields the following modification of equation (58):

$$T_{i,j}^{(new)} = \omega\, T_{i,j}^{(new)(58)} + (1 - \omega)\, T_{i,j}^{(old)} \tag{59}$$

where $T_{i,j}^{(new)(58)}$ is calculated from (58). The parameter ω is known as the over-relaxation parameter, and accelerates convergence when $1<\omega<2$. The optimum value for ω varied from time level to time level, and was determined empirically. For the standard composite blade construction,

it was found that the optimum ω was about 1.7 for times less than 5 sec., 1.5 for times between 5 and 15 sec. and 1.3 for times greater than 15 sec. If the phase change is not considered, the ice layer can be treated as the IIth layer of the blade, and over-relaxation is used for this layer also.

The total number of calculations made can also be reduced by increasing the time step Δt as the calculations proceed. When ice shedding occurs, however, the rapid change in temperature requires the standard time step of 0.10 sec. to be reduced to 0.001 sec. in order for accurate results to be obtained.

For more information on the methods used in the formulation and implementation sections, see References 10 and 11.

B. COMPUTER PROGRAM AND ALGORITHM

The complete program listing appears in the Appendix along with a sample input data file. The first eighty lines define the program input variables and their English units. The program can accept data in any consistent set of units, as only the input-output formats need be modified. A metric version of the program has been compiled and is available upon request.

The flow chart for the main program is shown in Figure 4. Dashed boxes may be skipped depending on the problem being solved. The subprograms used in the computer program have the following function: STEP determines the new time

step and adjusts time dependent parameters; SOURCE determines the value of the source term at a half-time step; CONVE determines the percent difference between a new and old nodal temperature during an iteration; WLAYER calculates the temperatures and enthalpies in the ice-water layer using the Enthalpy method; and PHASE determines the phase of a node and sets phase dependent properties. Figure 5 is the flow diagram for the subprograms WLAYER and PHASE, and illustrates the details of the determination of whether or not a given node is solid, liquid or melting.

V. DISCUSSION OF RESULTS

The computer model developed in this investigation was used to study the effects of a number of design parameters on de-icer performance. These included the effects of heater power density and thickness, imperfect contact between layers, initial ice layer thickness, variable heater output, phase change in the ice layer and shedding of the ice. As stated previously, de-icer performance is measured by the time required to melt some specified thickness of ice at the abrasion shield-ice interface, starting from various initial composite blade temperatures. This time is referred to as the de-icing time; when it is reached, the ice can be shed by the dynamic forces acting on the outer surface of the composite blade. If the specified thickness of ice is zero, then the de-icing time is equal to the time required to raise the abrasion shield-ice interface temperature to 32°F. To determine the zero thickness de-icing time, the phase change in the ice layer need not be considered. The phase change is not considered in Parts A through F below. Parts G through K require use of the Enthalpy method for the phase change. All figures and tables referred to below appear on pages 59 through 85. In addition to performance curves, temperature

response curves and profiles for some of the cases studied are presented and a comparison with experimental data is made.

A schematic drawing of a composite aircraft blade on which an ice layer has formed appears in Figure 1a. Figure 1b shows the one-dimensional finite difference grid used in the simulation and lists the number of nodes used in each layer for the standard de-icer design studied. These node numbers were enough to ensure that accurate solutions were obtained. Material property data and design data for the standard de-icer appear in Tables 1a and 2a, respectively. Any variations from this design are clearly marked on all graphs presented.

A. Verification of Finite Difference Method

In order to verify the use of the Crank-Nicolson finite difference equations in the computer simulation, a problem for which an analytical solution existed was run. The problem chosen was to determine the temperature distribution in an infinite slab of thickness 2b as a function of time, when the slab was initially at a temperature T_o and the surfaces of the slab were suddenly raised to a constant temperature T_1. The analytical solution for the problem is [12]:

$$\frac{T - T_o}{T_1 - T_o} = 1 - 2/\pi \sum_{n=0}^{\infty} \frac{(-1)^n}{(n+1/2)} \exp\left[-(n+1/2)^2 \pi^2 \alpha t/b^2 \right] \cdot$$

$$\cos\left[(n+1/2)\pi y/b\right]$$

The comparison between the analytical and numerical solutions appears in Figure 6. In this graph, the dimensionless temperature, $\frac{T - T_o}{T_1 - T_o}$, is plotted as a function of the dimensionless distance, y/b, and the dimensionless time, $\alpha t/b^2$. The analytical solution was obtained by summing a large number of terms in the infinite series. The comparison is very good, with only a slight discrepancy occurring for large times. A variable time step, which increased with time, was used in the simulation to achieve this accuracy.

Baliga [1] also used the Crank-Nicolson finite difference scheme in his simulation. He compared the analytical and numerical solutions for a two layer slab problem and obtained equally good results.

B. Effect of Power Density

Figure 7 shows the effect of heater power density on de-icer performance. As with all performance graphs to follow, the temperature rise, which is the difference between the melting point of ice and the initial temperature, is plotted on the ordinate and the de-icing time is plotted on the abscissa. The power density curves computed ranged from 15 to 40 Watts/in^2. These curves were also calculated by Baliga [1] and Stallabrass [2] with their computer models. There is perfect agreement between the results from this study and that of Baliga. This is expected since the phase change in the ice layer is not considered. Stallabrass' results tend to be slightly optimistic in comparison. The

curves shown in Figure 7 verify the observation made from experiments that the acceptable minimum power density is about 25 Watts/in^2. The de-icing time increases rapidly as the power density is reduced, especially at low initial temperatures.

C. Effect of Heater Thickness

Heater thicknesses vary drastically depending on whether the heater is a woven mat of wires and glass fibers or a resistance ribbon. Woven mats are an order of magnitude thicker than ribbons. Figure 8, however, shows that the heater thickness does not greatly affect de-icer performance, as the maximum difference between the de-icing times for the thicknesses shown is less than 1 sec. Curve 1 is for a point (zero thickness) heater. This is an idealization which shows the best possible results attainable. Curves 2 and 3 are for thicknesses characteristic of resistance ribbons, and curve 4 is for thicknesses characteristic of woven mats.

D. Effect of Imperfect Contact between Layers

The layers that make up a composite aircraft blade are held together by thin layers of epoxy resin. In addition, small air gaps may exist that cause poor contact between adjacent layers. These factors give rise to a resistance tc heat transfer across the layer interfaces. This resistance can be accounted for by means of an interfacial heat transfer coefficient. Figure 9 shows the effect of imper-

fect contact between layers on de-icer performance. The same heat transfer coefficient was assumed for all interfaces in the blade, and perfect contact was assumed at the abrasion shield-ice interface. An infinite heat transfer coefficient corresponds to perfect contact. The results indicate that imperfect contact has little effect on performance down to a coefficient of about 500 Btu/ft^2-hr-°F. Then, a drastic decrease in performance occurs between 500 and 100 Btu/ft^2-hr-°F, with de-icing times increasing by as much as 3 sec. The former coefficient corresponds to a resin thickness of approximately 0.005", and the latter to a thickness of approximately 0.01". This rather drastic change has not been accounted for in the previous investigations surveyed.

E. Effect of Initial Ice Layer Thickness

In Figure 10, the effect of the ice thickness present when the heater is turned on is shown. The thicknesses studied ranged from 0.1" to 0.5". One might expect that the de-icing time would increase as the thickness of the ice layer is increased, but the opposite is true. The ice acts as a layer of insulation, so that the abrasion shield-ice interface temperature rises faster for thicker ice layers. For thin ice layers and high convection at the ice-ambient interface, the heat is rapidly conducted away from the abrasion shield-ice interface. In fact, the initial ice layer thickness has a greater effect on de-icer performance than any of the parameters previously discussed.

The curve for 0.1" of ice clearly shows that for low initial temperatures, thin layers of ice cannot be effectively removed with a power density of 25 Watts/in^2. That the effect of the initial ice layer thickness has an upper limit can be seen by comparing the curves for 0.5" and 0.25" of ice. They are nearly identical.

F. Effect of Variable Heater Output

A variety of time-dependent heater outputs can be specified in the computer simulation. These are given in the "Numerical Formulation" section. A comparison was made between a heater with a sinusoidal output and a heater with a constant output of 25 Watts/in^2. For simplicity, the phase change was not considered. The sinusoidal heater output that was studied is given by:

$$q(t) = 25\ [\ 1 + \cos(\pi/2t - \pi)\ ]$$

It has an average power density of 25 Watts/in^2 and a period of 4 sec. The de-icing time starting from an initial temperature of -4°F was found to be slightly longer for the sinusoidal heater output, being 5.7 sec. compared to 4.9 sec. for the constant heater output.

The temperature responses for the substrate, heater, abrasion shield-ice interface and ice-ambient interface are shown in Figure 11 for both heater outputs. For these response curves and those that follow in this section, the temperature variations across the substrate, heater and abrasion shield were usually much less than 1°F. The

sinusoidal heater output responses for the heater and the abrasion shield-ice interface oscillate, with different amplitudes and time lags, around the constant heater output responses. The substrate response, however, oscillates only slightly and is essentially superimposable with the constant heater output response. The temperature at the outer surface of the ice remains constant at -4°F. This is due to the large heat transfer coefficient at this surface.

G. Application of the Enthalpy Method

When the Enthalpy method is applied as described in the "Numerical Formulation" section, temperature responses like those shown in Figure 12 result. Figure 12 shows the abrasion shield-ice interface temperature response for the standard de-icer design with a heater output of 25 Watts/in^2 and an initial temperature of -4°F. The response behaves unrealistically after melting begins. Above 32°F, the temperature oscillates with a frequency which is nodal dependent. This can be seen by comparing the two curves for 20 and 60 nodes in the ice layer. The broken curve is the temperature response predicted with the computer model of Baliga [1], and it also shows this behavior. These oscillations have been attributed to the fact that, when the Enthalpy method is used, a node in the ice layer remains at the melting point for a finite period of time.

Figure 12 shows that Baliga's curve compares well in magnitude with those from the present study. The 3°F

difference which occurs after melting has begun is due to the fact that Baliga [1] approximates the latent heat effect with a large change in heat capacity over a 1° interval around 32°F. The Enthalpy method does not require this approximation.

Voller and Cross [8,9] have shown, by comparing analytical and numerical solutions to simple phase change problems, that numerical solutions based on the Enthalpy method oscillate around the true solutions. They have also derived a criteria for determing the points of correspondence between the true and oscillating solutions. By finding these points of correspondence, accurate response curves can be obtained. It was shown in Section III, Part D, that the nodal enthalpy, $H_{w,j}$, could be directly related to the fraction of the node melted, Y_j, when the node was at the melting point. When $Y_j = \frac{1}{2}$, the liquid-solid interface is exactly at node j. It is when this occurs that the true and oscillating curves agree. By plotting the response variable when $Y_j = \frac{1}{2}$ at successive nodes, accurate response curves can be obtained.

The above procedure was used to replot the 20 and 60 node curves in Figure 12, as well as to plot data for 30, 40 and 90 nodes in the ice layer. The result is shown in Figure 13. The temperature response curve is now physically realistic and has very little nodal dependence. Thirty nodes was found to be the practical minimum number of nodes, and 30 nodes per every 0.25" of ice were used in all the results that follow.

Also, in all the graphs that consider melting in the ice layer, the points of correspondence obtained from the plotting procedure of Voller and Cross are clearly marked. The discontinuity in the slope which occurs when the abrasion shield-ice interface reaches the melting point of 32°F is characteristic of phase change problems.

Also plotted in Figure 13 is the abrasion shield-ice interface temperature obtained with the approximation of equal liquid water and solid ice thermal conductivities. It is clear from Figure 13 that this is a bad assumption. In reality, liquid water has a lower thermal conductivity than ice. Thus, the thin layer of water which forms when the ice melts acts as an additional layer of insulation. This is the reason the true response curve lies above the approximate curve in Figure 13.

It was found that the method of averaging used for the thermal conductivity between adjacent nodes in the ice layer significantly affected the numerical results. Only when a continuous volume average between adjacent nodes was used did the plotting procedure of Voller and Cross eliminate all nodal dependence. Volume averaging gives the correct values for $k_{w,j-1/2}$ and $k_{w,j+1/2}$ when the liquid-solid interface is exactly at node j (see Section III, Part D).

H. Effect of Phase Change

The graphs discussed here are for the same set of conditions as were used for Figures 12 and 13.

Figure 14 shows the temperature responses for the substrate, heater, abrasion shield-ice interface and ice-ambient interface. Also plotted are the responses obtained without considering the phase change in the ice layer. The absorption of the latent heat during melting has the effect of lowering the temperatures in the composite aircraft blade after melting begins at 4.9 sec.

The ratio of computing time to simulation time was 0.9 without the phase change and 1.5 with the phase change on the University of Toledo IBM 4341 computer. For comparison, Baliga's [1] computing times for the same problem were approximately five times longer (however, 60 nodes was the minimum number of nodes used in the ice layer). This difference is partially due to the complexities of the matrix inversion technique used by Baliga.

Figure 15 contains two temperature profiles across the composite blade-ice body. The profile for 4.0 sec. is before melting begins, and the profile for 16.3 sec. is after a thin layer of ice has melted. The slight gradients across the substrate, heater and abrasion shield that were mentioned earlier are apparent. The profile after melting has begun contains an extra segment (#6) corresponding to the thin water layer which has formed next to the abrasion shield.

The movement of the liquid-solid interface is plotted in Figure 16. The plotting procedure of Voller and Cross was also used for this response. For comparative purposes,

the curve for equal thermal conductivities and the curve predicted by Baliga's simulation [1] are shown. Baliga predicts a slightly longer abrasion shield-ice interface melting time than the present investigation, 5.5 sec. as compared to 4.9 sec. This is due to the approximate phase change technique used by Baliga.

To directly consider the effects of heater element gaps on de-icer performance requires a two-dimensional model. This is because a finite thickness of ice will melt above the heater before any ice melts above the heater gaps. However, this effect can be studied indirectly by defining the de-icing time as the time required to melt different thicknesses of ice at the abrasion shield-ice interface. This is done in Figure 17. The curve for 0" of ice is the same as the 25 Watts/in^2 curve in Figure 7. The other curves are for the different thicknesses of ice that must be melted for de-icing. They show the general increase in de-icing time with required thickness for de-icing.

I. Comparison with Experimental Data

Since the de-icer problems considered in this study cannot be solved analytically when the phase change is taken into account, a comparison of the numerical results obtained from the computer simulation with experimental data was made. Gent and Cansdale [3] present temperature data measured from three laboratory de-icer pads. The

material property data for these test specimens appears in Table 1b. The design data appears in Tables 2b, c and d.

Table 3 contains the numerical and experimental melting times for the abrasion shield-ice interface. The experiments were run for the three different de-icer pads at three different heater power densities, 16.6, 19.0 and 22.5 Watts/in^2. The initial temperature in all cases was 4.1°F. The ice layer was 0.1" thick and twelve nodes were used in this layer. It can be seen in column 3 that when perfect contact between layers is assumed in the computer model, the predicted melting times are about 1 sec. too short. Gent and Cansdale [3] give the thicknesses for the glue between layers as between 0.001" and 0.002". This enabled the interfacial heat transfer coefficient to be estimated at between 600 and 1200 Btu/ft^2-hr-°F. These values were determined by dividing the thermal conductivity of epoxy resin by the glue thicknesses. The ranges for the melting times obtained using these heat transfer coefficients had a span of a few tenths of a second and appear in the fourth column of Table 3. Almost all of the experimental data lies within these ranges.

To further compare the numerical results from the computer simulation with experimental data, the abrasion shield temperature responses for all three specimens with 16.6 Watts/in^2 were plotted. These curves are shown in Figure 18. Prior to the onset of melting the discrepancies

between the numerically predicted and experimental temperature data are less than 2°F. After melting begins, the temperature rises predicted by the computer model are too optimistic. The best comparison is for specimen 3. Considering the experimental difficulties encountered by Gent and Cansdale (Appendix of Reference 3), the agreement is still very good.

J. Effect of Ice Shedding

In actual operation, when the de-icing time is reached, the ice layer plus any water which has formed is shed by the dynamic forces acting on the outer surface of the blade. Then, once the heater has been turned off, a new ice layer may form. For this reason, the heater is turned on and off periodically. This process was simulated with the computer model by shedding the ice layer at the de-icing time and then, after a period of time, adding a new ice layer. The de-icing time was taken to be the time required to raise the abrasion shield-ice interface temperature to 32°F. The ice was replaced every 20 sec., and the heater was turned on for 10 sec. and then off for 10 sec. The temperature responses for the various locations in the composite aircraft blade are shown for the first 20 sec. cycle in Figure 19. A sharp decrease in the heater temperature occurs at 4.9 sec. and 10 sec. The first decrease is from the ice being shed, and the second is from the heater being turned off. The abrasion shield outer surface temperature drops immediately from 32° to −4°F when the ice

is shed. Within 4 sec. of the heater being turned off, all the layers above the inner insulation have cooled to within 4°F of the initial temperature. Only the substrate remains hot after 20 sec. The time step had to be reduced drastically to follow the rapid change in temperatures which occurred when the ice was shed.

The second cycle, from 20 to 40 sec., is shown in Figure 20. The responses are quite similar to those in Figure 19. The only significant difference is the substrate temperature which is hotter. The de-icing time decreased to 4.5 sec. The cyclic process was continued until a steady value of 4.4 sec. was obtained for the cyclic de-icing time. Thus, the difference between the first cycle de-icing time and the steady value is only 0.5 sec. It is apparent that the temperature distribution present when the heater is turned on does not greatly affect de-icer performance. This is because once the ice is shed, heat is lost rapidly through the abrasion shield outer surface.

K. Effect of Refreezing

It is desirable to see what the temperature responses would be like if the ice layer could not be shed within the 10 sec. heating time allotted in Part J. Figure 21 shows the temperature responses for this case. When the heater is turned off, the temperatures in the heater and abrasion shield drop immediately, with the heater temperature drop-

ping below the abrasion shield-ice interface temperature after 13.3 sec. Quite surprisingly, the water begins to refreeze at the abrasion shield outer surface after only 14.5 sec. The computed temperature profile data reveals that this is not due to the complete refreezing of the water, but to the formation of a second ice layer. Thus, the water layer is sandwiched between two layers of ice. After 19.9 sec., the water has completely refrozen.

VI. CONCLUSIONS AND RECOMMENDATIONS

The one-dimensional electrothermal de-icer pad computer simulation developed in this study has been shown to predict accurate and consistent temperature distributions and ice-water interface location information. The accuracy was checked by comparing computed results with analytical solutions and experimental data. The simulation contains the following improvements over previous simulations on the subject:

1) The Crank-Nicolson finite difference scheme was used instead of the forward finite difference scheme. This reduced the total number of calculations that must be done by allowing a larger time step to be used. Round-off error was also decreased;
2) The Enthalpy method was used for the phase change occurring in the ice layer. This method is more direct and easier to apply than methods previously used;
3) The iterative method of solution used and the computer program algorithm can easily be extended to handle two-dimensional problems; and
4) Many of the restrictions placed on previous simulations were removed. These restrictions included

perfect contact between layers in the composite aircraft blade and no consideration of the phase change in the ice layer. The present simulation can also consider a variety of boundary conditions, variable heater outputs and shedding of the ice layer.

Further simulation work in the field of electrothermal de-icing should focus on the development of a two-dimensional computer model, so that the effect of heater gaps and blade geometry on de-icer performance can be rigorously studied. This work is currently under way in the Chemical Engineering Department of the University of Toledo. In addition, a complete experimental study should be made on real de-icer pads. This would enable such parameters as heat transfer coefficients and layer thicknesses to be determined more accurately. It would also serve as a check on the assumptions used in the computer model. Finally, work should be initiated to determine and characterize the mechanism of ice deposition on aircraft surfaces.

REFERENCES

1. Baliga, G., "Numerical Simulation of One-Dimensional Heat Transfer in Composite Bodies with Phase Change," M.Sc. Thesis, Univ. of Toledo, Toledo, Ohio, 1980.

2. Stallabrass, J. R., "Thermal Aspects of De-Icer Design," presented at The International Helicopter Icing Conference, Ottawa, Canada, 1972.

3. Gent, R. W., and J. T. Cansdale, "One-Dimensional Treatment of Thermal Transients in Electrically De-Iced Helicopter Rotor Blades," RAE Technical Report 80159, 1980.

4. Campbell, W. F., "A Rapid Analytical Method for Calculating the Early Transient Temperature in a Composite Slab," NRC Lab Report MT-32, 1956.

5. Ockenden, J. R., and W. R. Hodgkins (editors), Moving Boundary Value Problems in Heat Flow and Diffusion. Oxford Univ. Press, Oxford, 1975.

6. Bonacina, C., Comini, G., Fasano, A. and N. Primicerio, "Numerical Solution of Phase Change Problems," Int. J. Heat & Mass Trans., 10, p. 1825, 1973.

7. Atthey, D. R., "A Finite Difference Scheme for Melting Problems Based on the Method of Weak Solutions," Moving Boundary Value Problems in Heat Flow and Diffusion. See Reference 5, p. 182.

8. Voller, V., and M. Cross, "Accurate Solutions of Moving Boundary Value Problems Using the Enthalpy Method," Int. J. Heat & Mass Trans., 24, p. 545, 1981.

9. Voller, V., and M. Cross, "Estimating the Solidification/Melting Times of Cylindrically Symmetric Regions," Int. J. Heat & Mass Trans., 24, p. 1457, 1981.

10. von Rosenberg, D. W., Modern Analytical and Computational Methods in Science and Mathematics. American Elsevier, New York, 1969.

11. Carnahan, B., Luther, H. A., and J. O. Wilkes, Applied Numerical Methods. Wiley, New York, 1969.

12. Bird, R. B., Stewart, W. E., and E. N. Lightfoot, Transport Phenomena. Wiley, New York, 1960, pp. 354-356.

Table 1. Thermal Properties of Selected Materials

Material (Use)	Thermal Conductivity		Heat Capacity		Density		Thermal Diffusivity	
	Btu / ft-hr-°F	W / m-°C	Btu / lb-°F	J / kg-°C	lb / ft³	kg / m³	ft² / hr	$10^5 \frac{m^2}{s}$
(a) Standard De-Icer Design								
(1) Aluminum Alloy 75S-T6 (Substrate)	66.5	115	0.23	963	175	2800	1.65	4.26
(2) Epoxy/Glass Filled 32% (insulation)	0.22	0.38	0.23	963	110	1760	0.0087	0.0225
(3) Nichrome 80/20 (heater)	7.6	13.2	0.107	448	515	8250	0.138	0.356
(4) Stainless Steel 304 (abrasion shield)	8.7	15.1	0.118	494	495	7930	0.15	0.387
(5) Water (32°F)	0.320	0.554	0.997	4174	62.4	999.6	0.0051	0.0132
(5) Ice (31° to 32°F, average)	1.416	2.45	0.502	2102	57.4	919.5	0.0492	0.127

Latent Heat of Fusion = 143.4 Btu/lb (333.6 kJ/kg)

Table 1. Thermal Properties of Selected Materials
(Continued)

Material (Use)	Thermal Conductivity		Heat Capacity		Density		Thermal Diffusivity	
	Btu / ft-hr-°F	W / m-°C	Btu / lb-°F	J / kg-°C	lb / ft³	kg / m³	ft² / hr	$10^5 m^2/s$
(b) Experimental Test Specimens								
(6) Aluminum Alloy (substrate)	98.2	170	0.230	963	175	2800	2.44	6.3
(7) GRP (insulation)	0.197	0.34	0.210	879	112	1800	0.0083	0.0215
(8) Constantan .6 Cu, .4 Ni (heater)	13.1	22.7	0.10	418	557	8920	0.235	0.607
(9) Nickel (abrasion shield)	52.58	91	0.109	456	556	8900	0.869	2.24
(10) Epoxy Resin (glue)	0.10	0.173	0.25	1050	75	1200	0.0053	0.0137
(c) Other Materials								
Aluminum (soft)	124	215	0.23	963	169	2705	3.20	8.26
Berylium Copper	60.5	105	0.10	419	515	8250	1.17	3.02
Copper	220	381	0.092	385	557	8900	4.29	11.1

Table 1. Thermal Properties of Selected Materials
(Continued)

Material (Use)	Thermal Conductivity		Heat Capacity		Density		Thermal Diffusivity	
	$\frac{Btu}{ft\text{-}hr\text{-}^\circ F}$	$\frac{W}{m\text{-}^\circ C}$	$\frac{Btu}{lb\text{-}^\circ F}$	$\frac{J}{kg\text{-}^\circ C}$	$\frac{lb}{ft^3}$	$\frac{kg}{m^3}$	$\frac{ft^2}{hr}$	$10^5 \frac{m^2}{s}$
(c) Other Materials (Continued)								
Titanium	13.3	23	0.082	343	281	4500	0.577	1.49
Glass ("E" Glass)	0.6	1.0	0.19	796	159	2550	0.020	0.052
Neoprene	0.108	0.187	0.295	1235	90	1440	0.0041	0.0105
Nylon	0.14	0.24	0.4	1675	70	1120	0.0050	0.013
Polytetrafluoro-ethylene (Teflon)	0.15	0.26	0.25	1047	138	2210	0.0043	0.011
Polytrifluoro-chloroethylene (KEL-F)	0.04	0.07	0.216	904	130	2080	0.0014	0.0036
Polyurethane	0.087	0.15	0.45	1885	75	1200	0.0026	0.0067
Ice (pure) 32°F	1.293	2.238	0.5057	2117	57.2	916.3	0.0445	0.115
14°F	1.356	2.347	0.5038	2109	57.3	917.9	0.0469	0.121
-4°F	1.416	2.451	0.5020	2102	57.4	919.5	0.0492	0.127

Table 2. De-Icer Pad Constructions

Layer	Material	Thickness in	Thickness mm	
(a) Standard De-Icer				
1	(1)	0.087	2.21	
2	(2)	0.050	1.27	$h_{a1} = 1.0 \frac{Btu}{ft^2\text{-}hr\text{-}^\circ F} \left(5.7 \frac{W}{m^2\text{-}^\circ C}\right)$
3	(3)	0.004	0.10	
4	(2)	0.010	0.25	$h_{a2} = 10^6$ (6×10^6)
5	(4)	0.012	0.30	
6	(5)	0.25	6.35	
(b) Test Specimen 1				
1	(6)	0.25	6.35	
2	(7)	0.015	0.38	$h_{a1} = 0$
3	(7)	0.005	0.125	
4	(8)	0.001	0.025	$h_{a2} = 1.76$ (10)
5	(7)	0.0075	0.19	
6	(7)	0.0075	0.19	$h_i = 600\text{-}1200$ (3400-6800)
7	(9)	0.015	0.38	
8	(5)	0.10	2.54	
glue layers	(10)	0.001 to 0.002	0.025 to 0.05	between 1-2,2-3,4-5,5-6,6-7

Table 2. De-Icer Pad Constructions
(Continued)

Layer	Material	Thickness in	Thickness mm	
(c) Test Specimen 2				
1	(6)	0.25	6.35	
2	(7)	0.070	1.78	h_{a1} = 0
3	(7)	0.005	0.125	
4	(8)	0.001	0.025	h_{a2} = 1.76 (10)
5	(7)	0.0075	0.19	
6	(7)	0.0075	0.19	h_i = 600-1200 (3400-6800)
7	(9)	0.015	0.38	
8	(5)	0.10	2.54	
glue layers	(10)	0.001 to 0.002	0.025 to 0.05	between 1-2,2-3,4-5,5-6,6-7
(d) Test Specimen 3				
1	(7)	0.30	7.62	
2	(7)	0.005	0.125	h_{a1} = 0
3	(8)	0.001	0.025	
4	(7)	0.0075	0.19	h_{a2} = 1.76 (10)
5	(7)	0.0075	0.19	
6	(9)	0.015	0.38	h_i = 600-1200 (3400-6800)
7	(5)	0.10	2.54	
glue layers	(10)	0.001 to 0.002	0.025 to 0.05	between 1-2,3-4,4-5,5-6

Table 3. Comparison of Experimental and Predicted Melting Times

	Heater Output ($Watts/in^2$)	Time to Melt (sec) Simulation*	Simulation†	Experimental
Specimen 1	16.6	7.9	8.6-8.9	9.0
	19.0	6.7	7.3-7.6	7.5
	22.5	5.4	6.0-6.3	6.3
Specimen 2	16.6	5.8	6.5-7.0	7.2
	19.0	5.0	5.7-6.2	5.8
	22.5	4.2	4.8-5.2	5.0
Specimen 3	16.6	5.8	6.6-7.1	7.3
	19.0	5.1	5.7-6.2	5.9
	22.5	4.2	4.8-5.3	5.0

*Assuming perfect contact between layers.

†With contact resistance between layers. The lower value is for $h_i = 1200 \frac{Btu}{hr\text{-}ft^2\text{-}^\circ F}$ (0.001" of glue), and the higher value is for $h_i = 600 \frac{Btu}{hr\text{-}ft^2\text{-}^\circ F}$ (0.002" of glue).

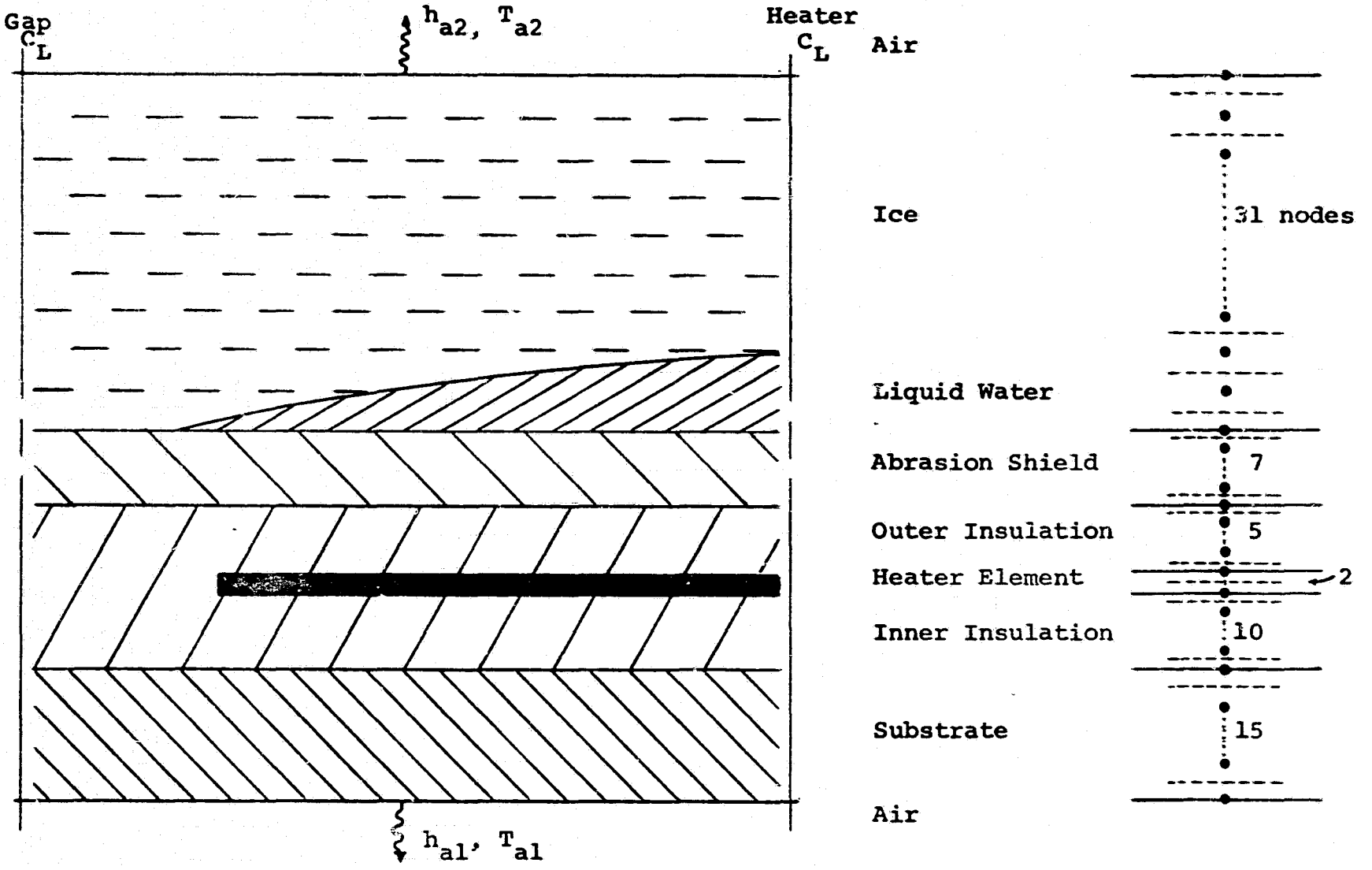

a) De-Icer Pad Construction

b) One-Dimensional Finite Difference Representation

Figure 1. Electrothermal De-Icer Pad Model

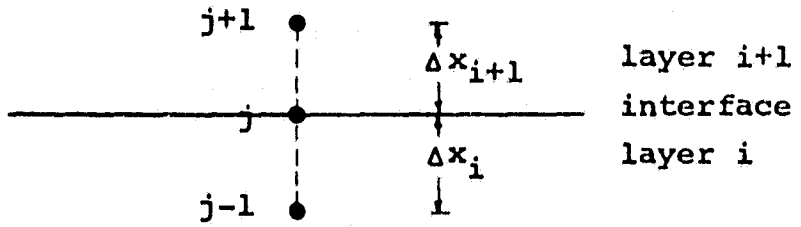

a) Perfect Contact Interface

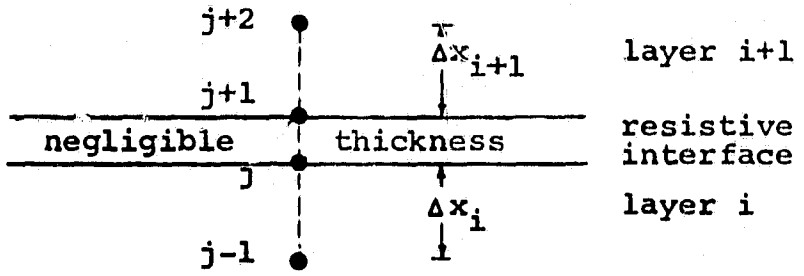

b) Resistive Interface

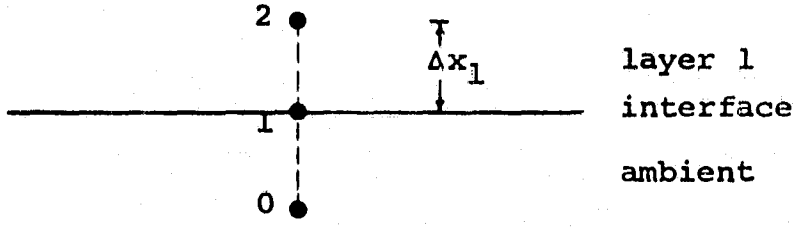

c) Inner Ambient Interface

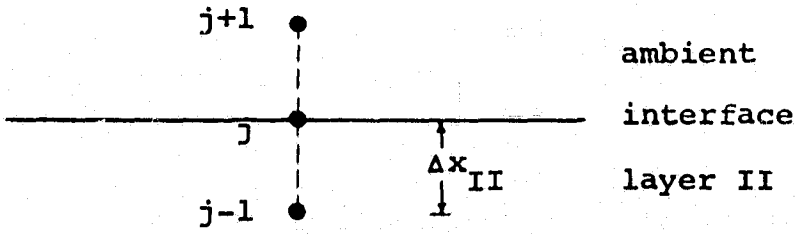

d) Outer Ambient Interface

Figure 2. Interface Finite Difference Grids

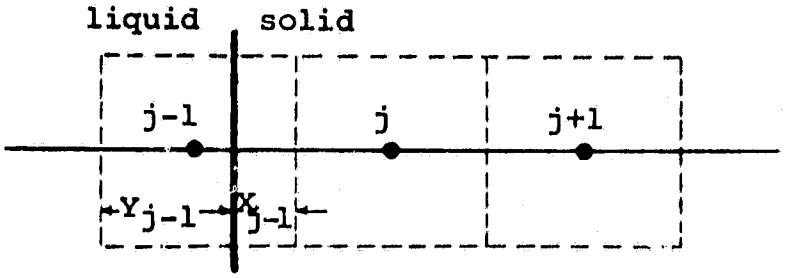

a) $k_{w,j-1/2} = [(Y_{j-1} - \frac{1}{2})k_l + (X_{j-1} + \frac{1}{2})k_s]$, $k_{w,j+1/2} = k_s$

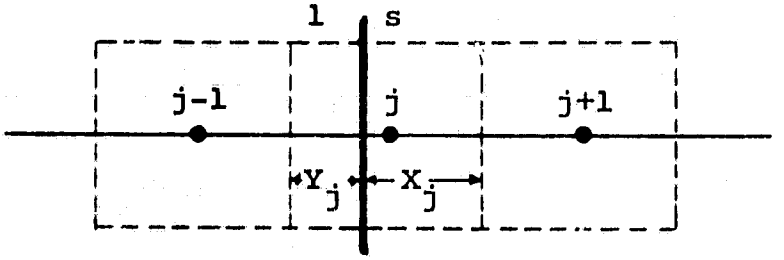

b) $k_{w,j-1/2} = [(Y_j + \frac{1}{2})k_l + (X_j - \frac{1}{2})k_s]$, $k_{w,j+1/2} = k_s$

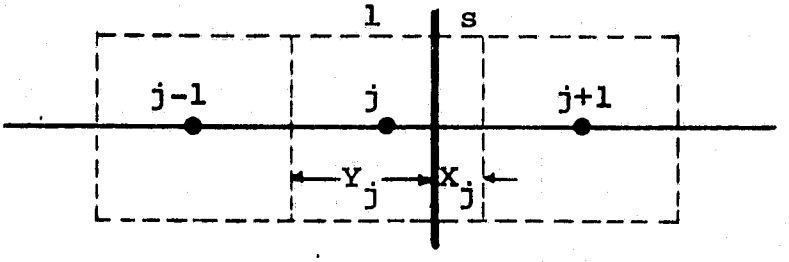

c) $k_{w,j-1/2} = k_l$, $k_{w,j+1/2} = [(Y_j - \frac{1}{2})k_l + (X_j + \frac{1}{2})k_s]$

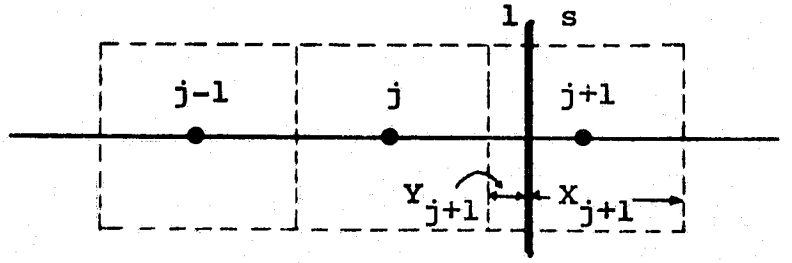

d) $k_{w,j-1/2} = k_l$, $k_{w,j+1/2} = [(Y_{j+1} + \frac{1}{2})k_l + (X_{j+1} - \frac{1}{2})k_s]$

Figure 3. Volume Averaging of k_w across the Liquid-Solid Interface

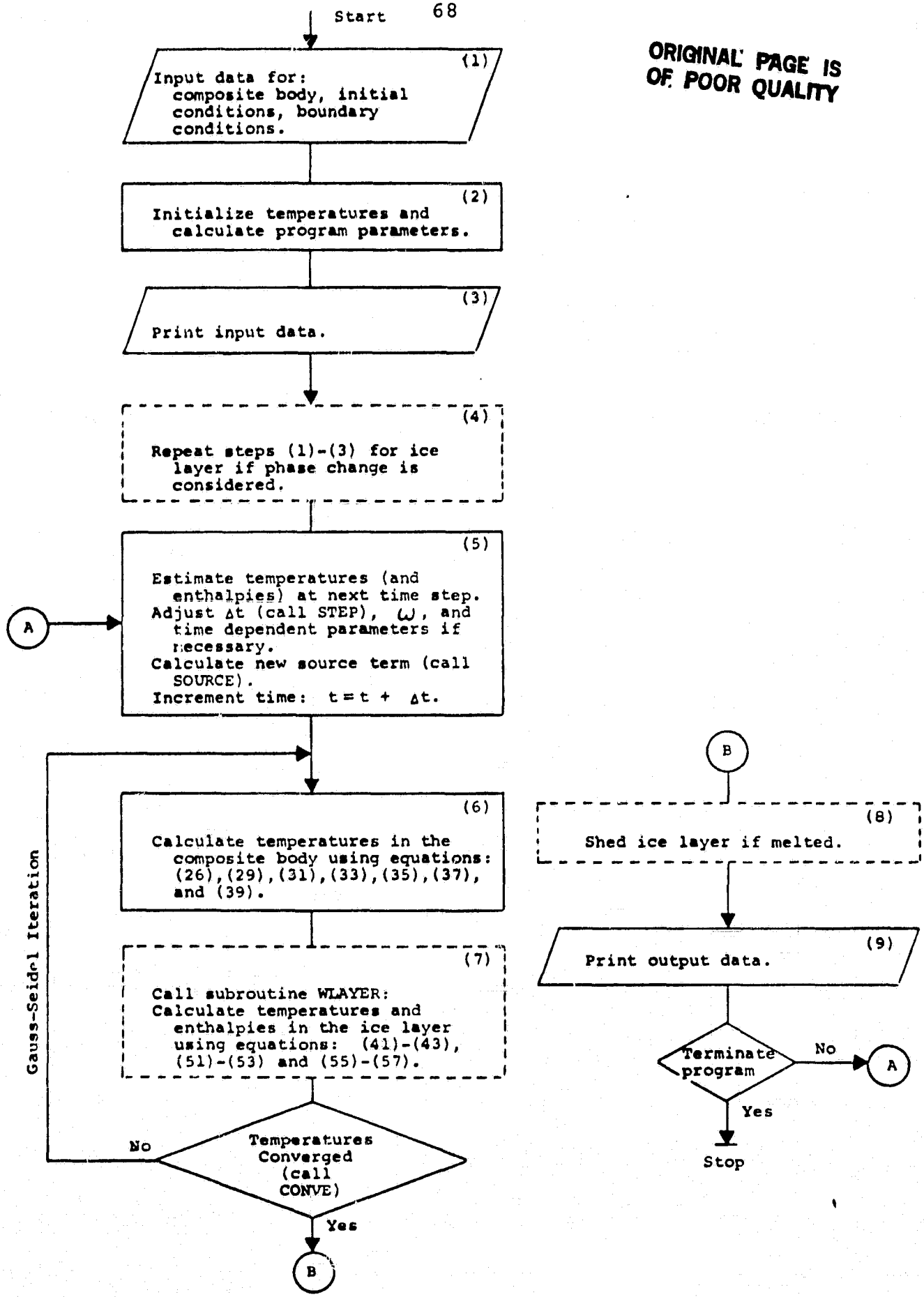

Figure 4. Flow Chart for Main Program

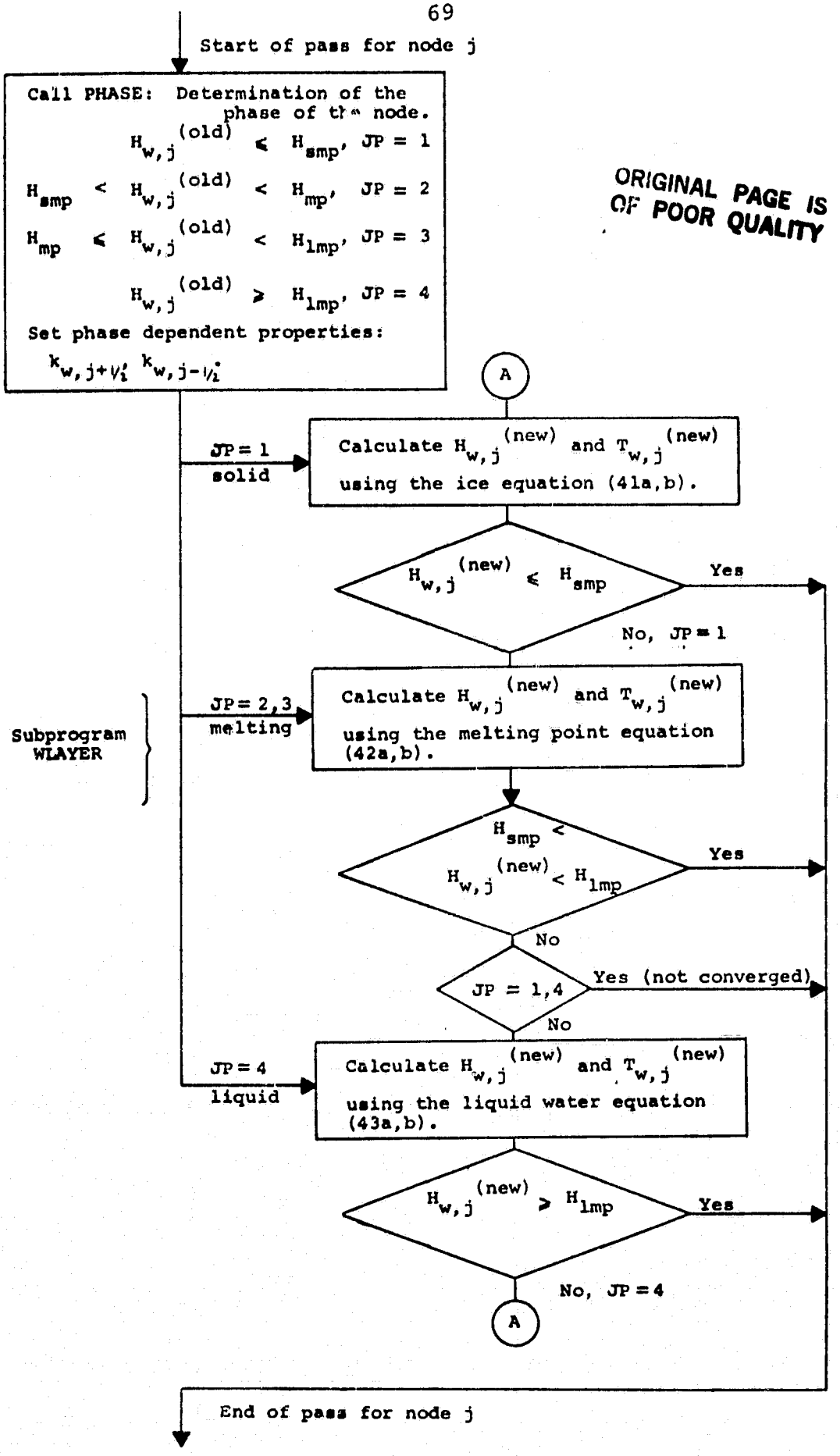

ORIGINAL PAGE IS OF POOR QUALITY

Figure 5. Flow Chart for Subprograms WLAYER and PHASE

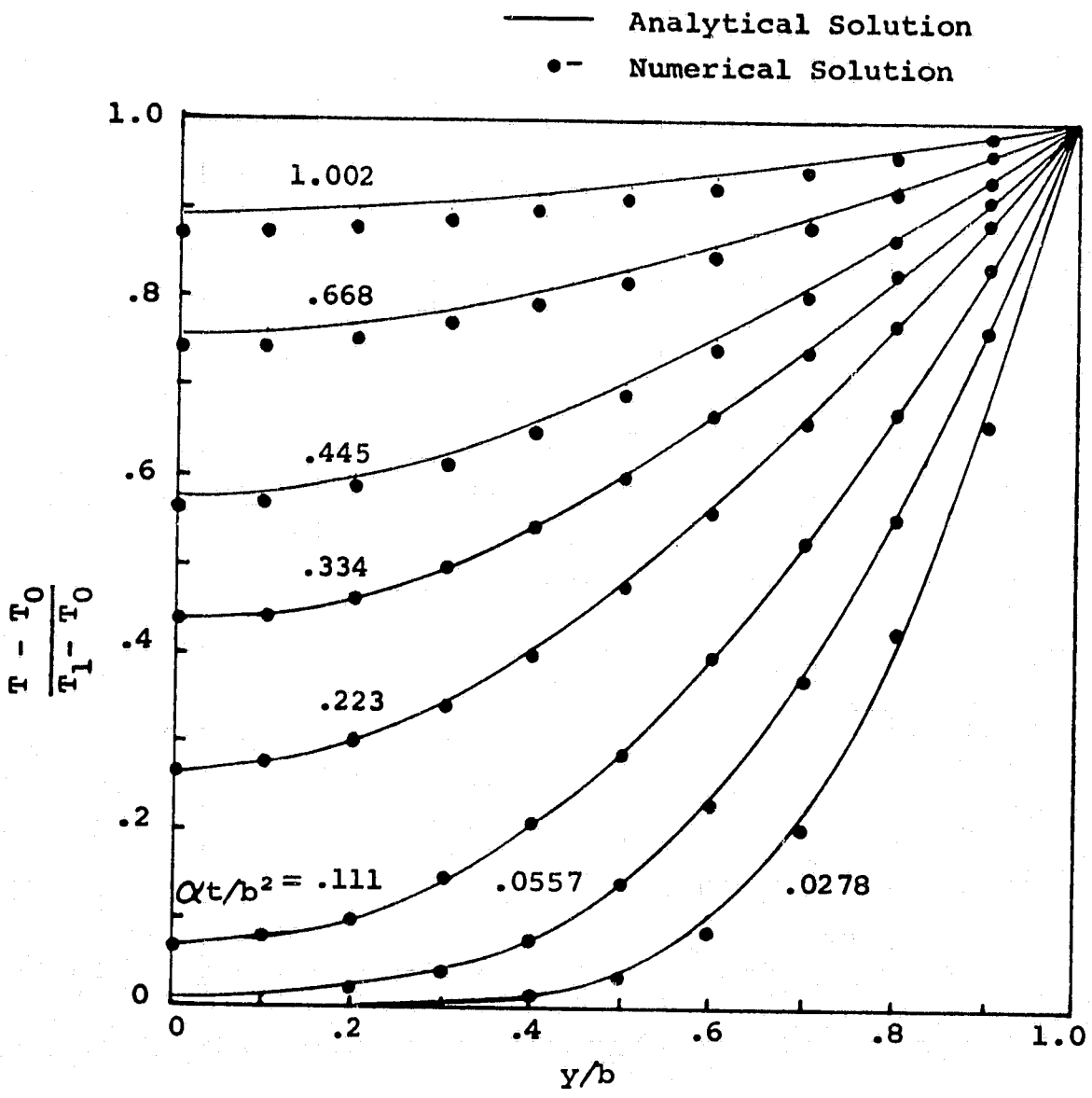

Figure 6. Comparison of Finite Difference and Analytical Solutions for Single Layer Problem

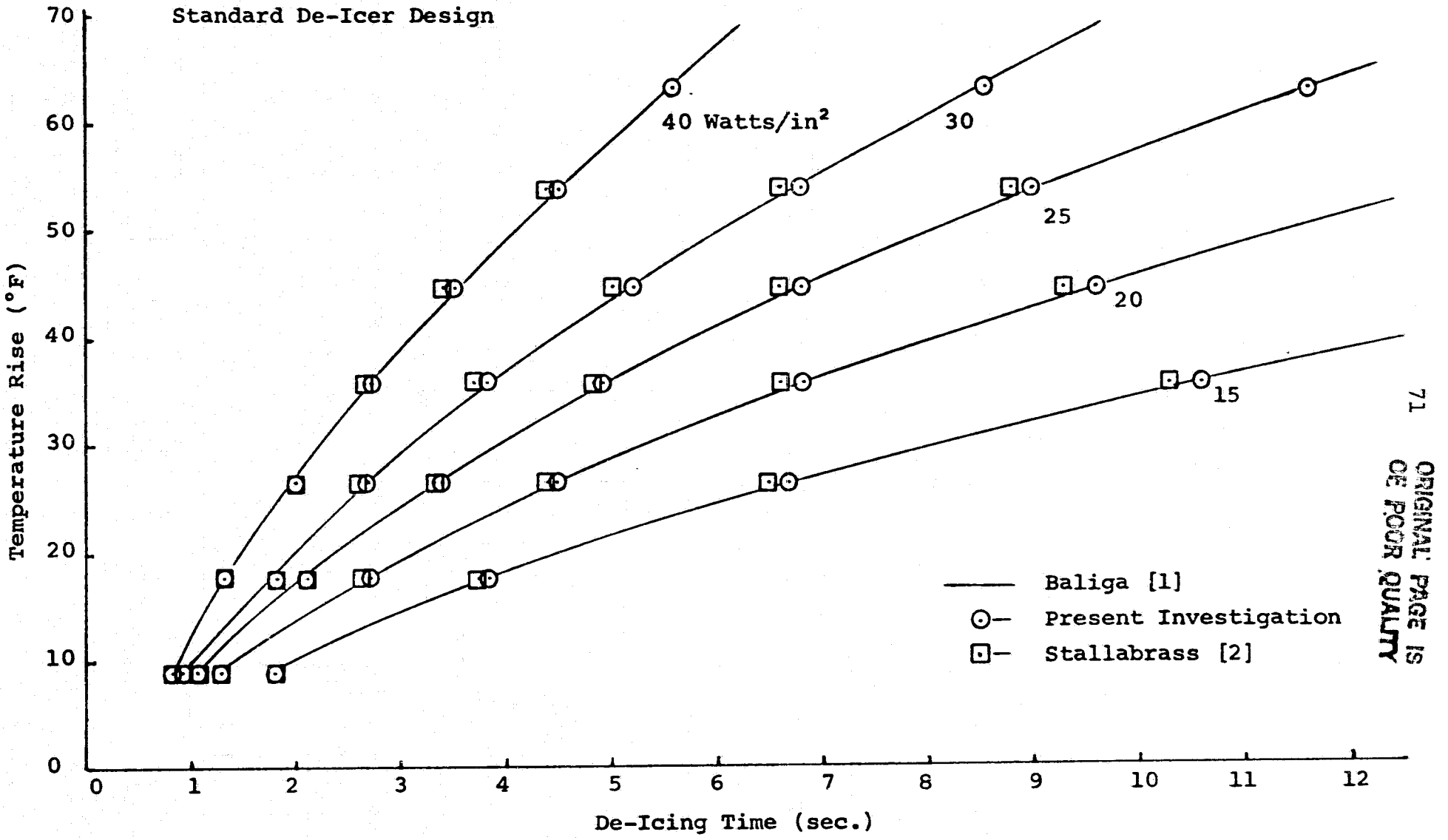

Figure 7. Effect of Power Density on De-Icer Performance

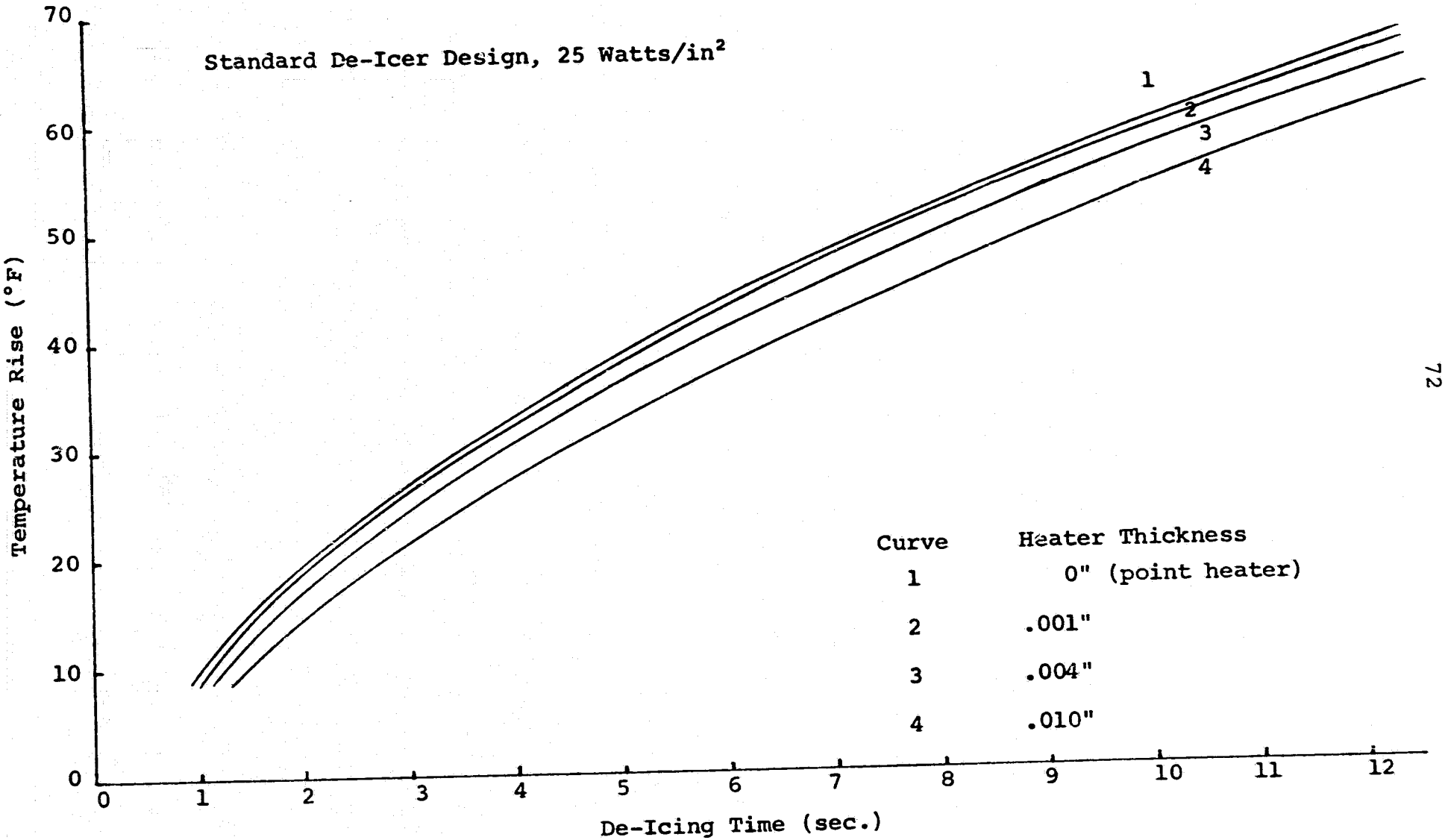

Figure 8. Comparison of Point and Finite Thickness Heaters

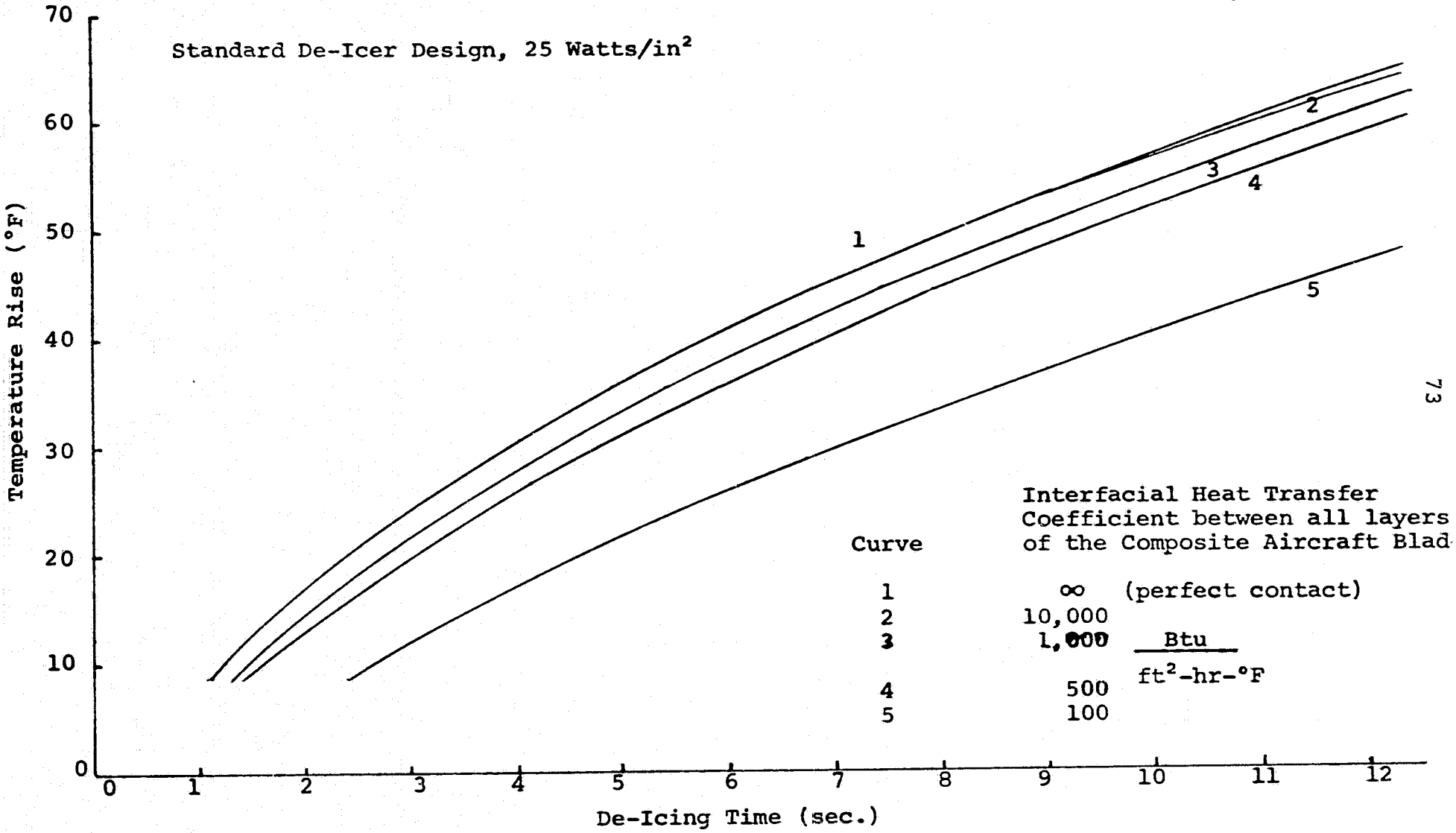

Figure 9. Effect of Imperfect Contact between Layers on De-Icer Performance

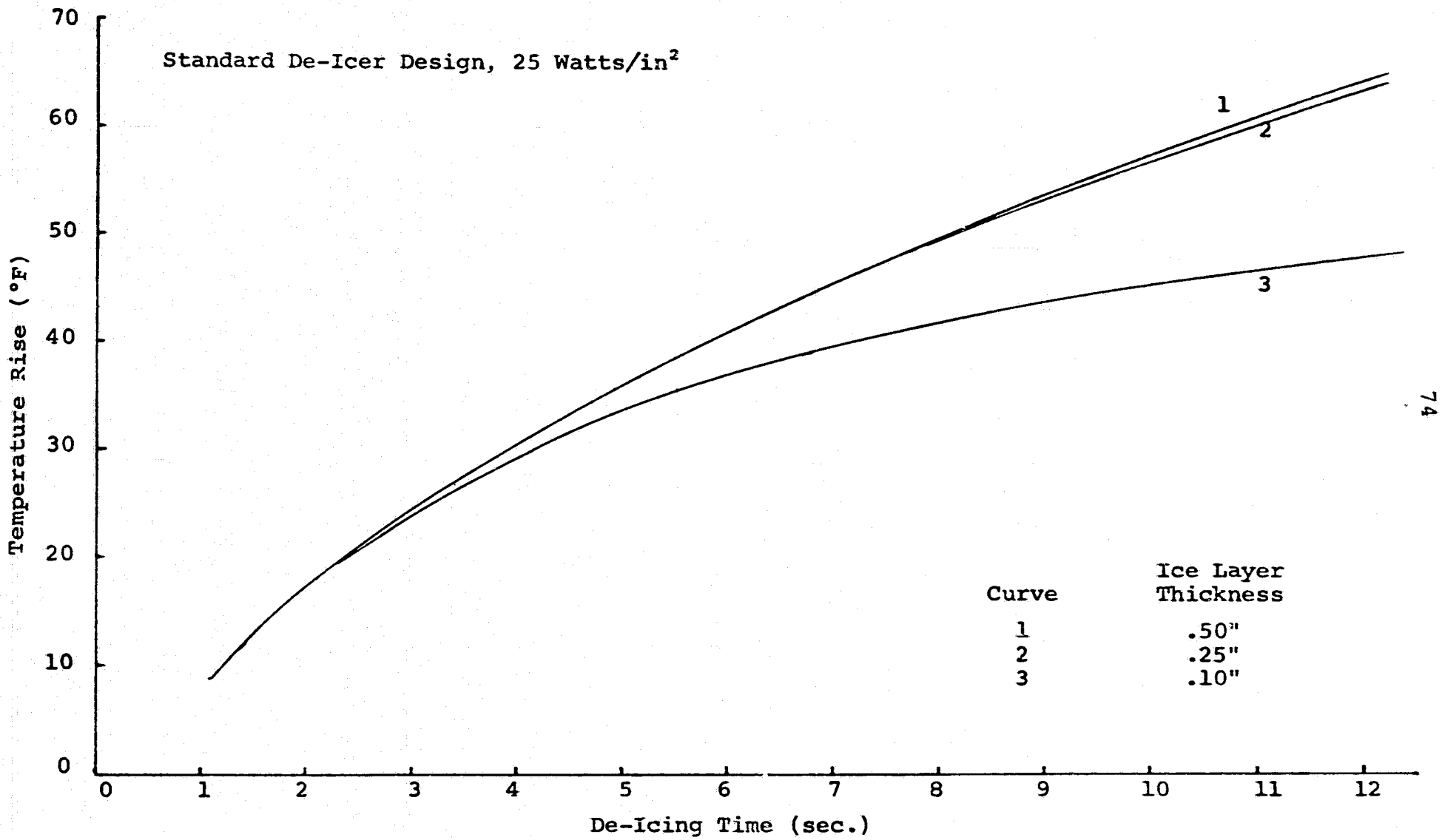

Figure 10. Effect of Initial Ice Layer Thickness on De-Icer Performance

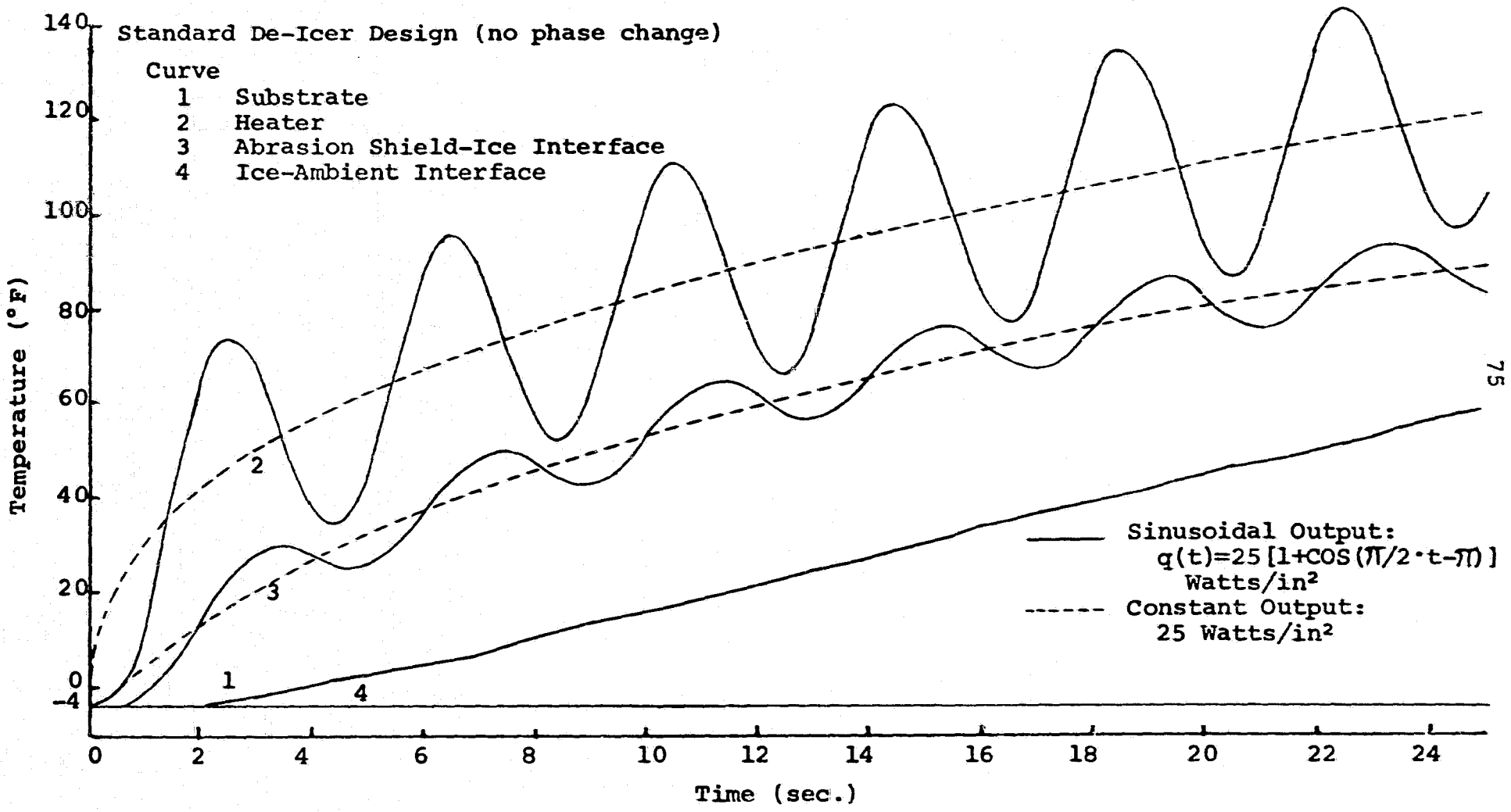

Figure 11. Comparison of Temperature Responses from Sinusoidal and Constant Heater Outputs

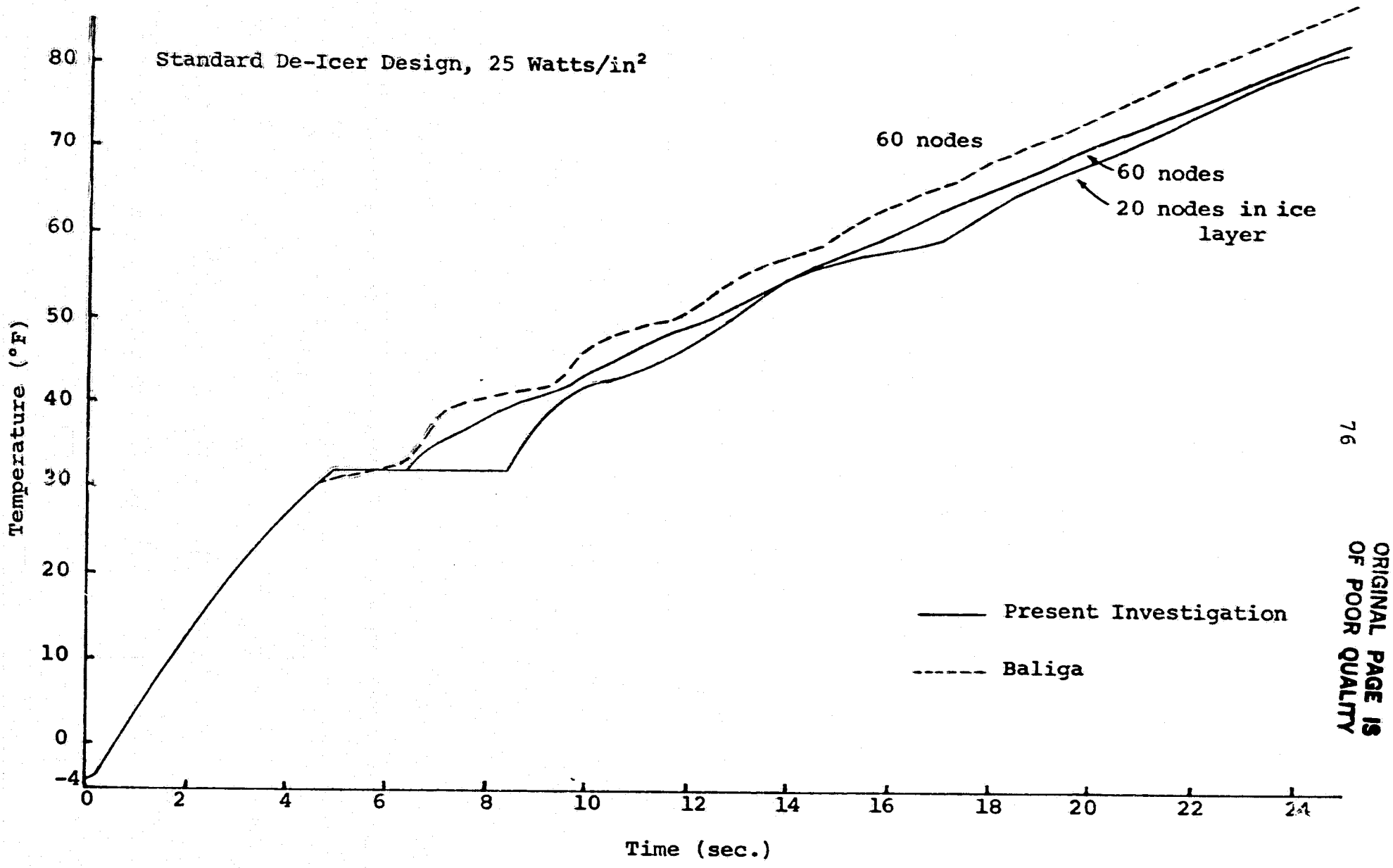

Figure 12. Abrasion Shield-Ice Interface Temperature with Phase Change

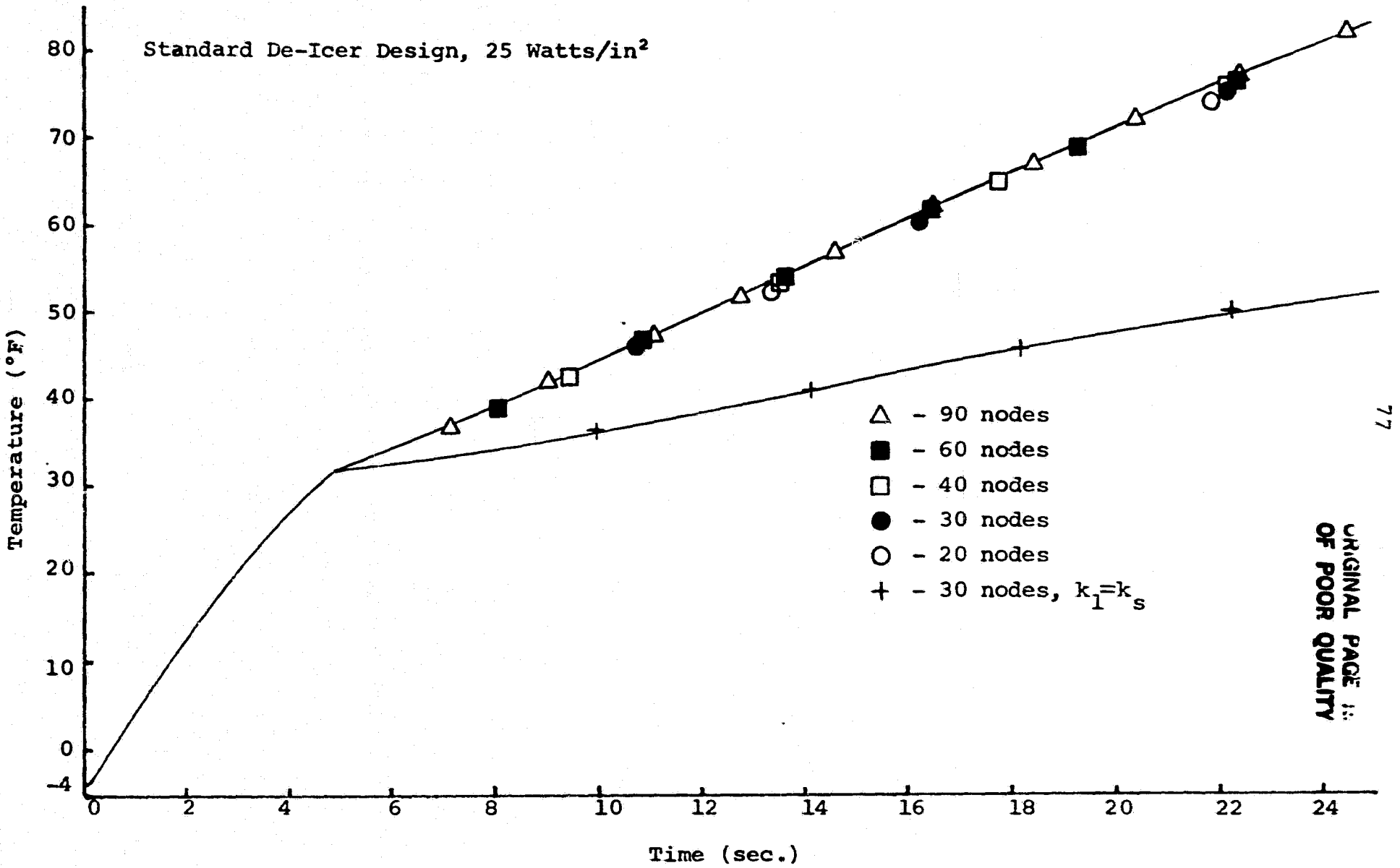

Figure 13. Abrasion Shield-Ice Interface Temperature following the Plotting Procedure of Voller and Cross

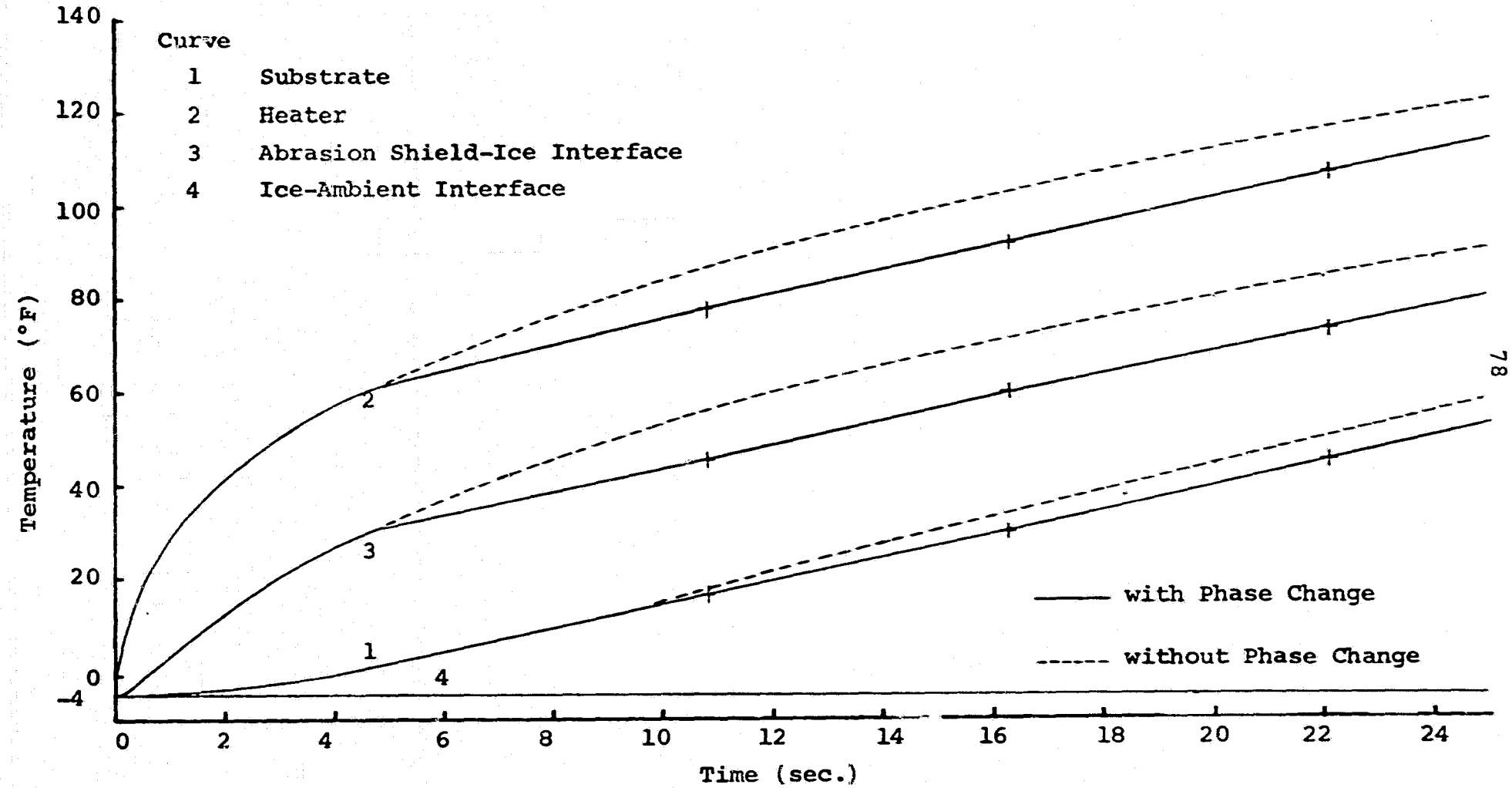

Figure 14. Temperature Response for Standard De-Icer Design Studied

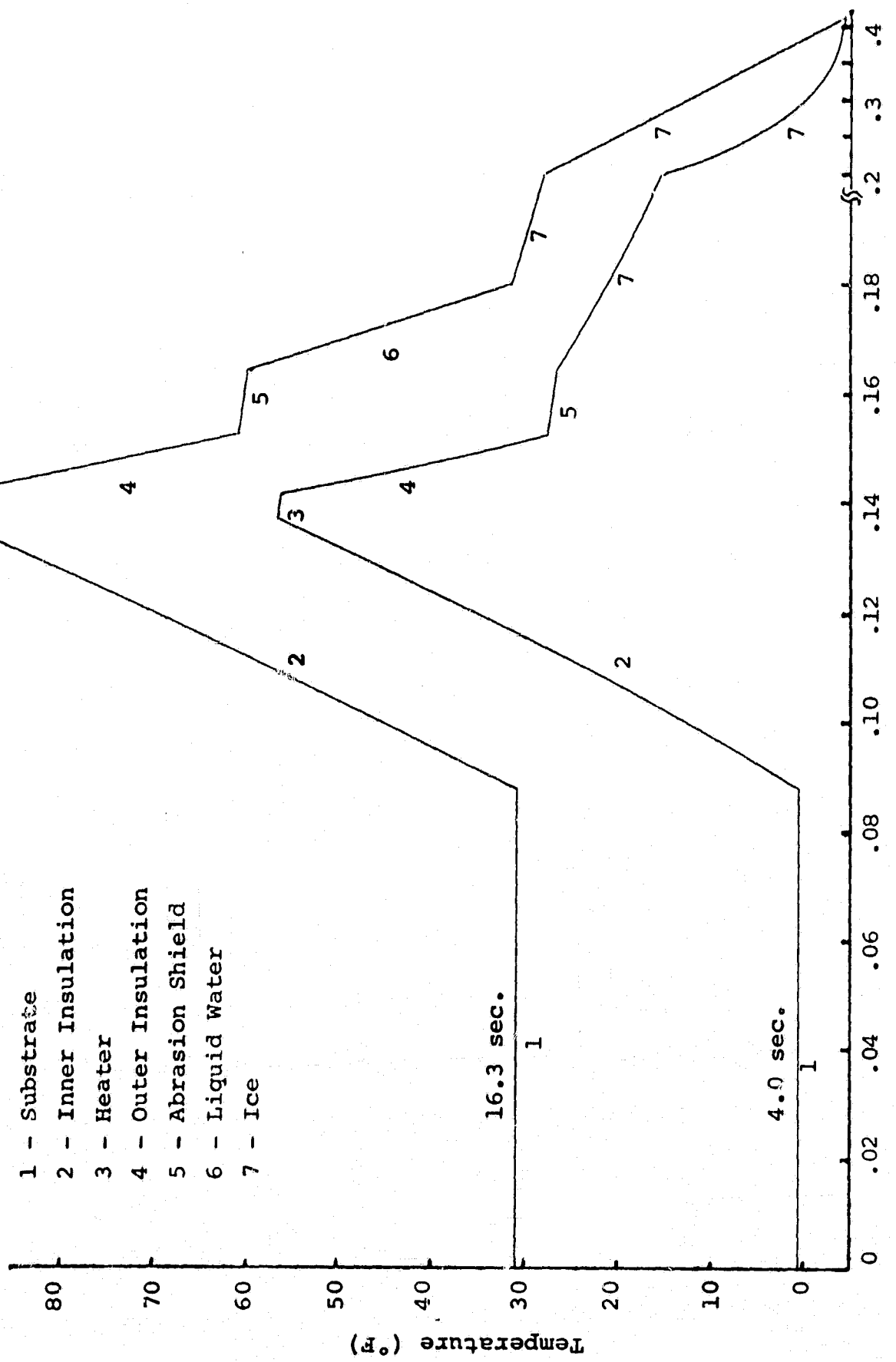

Figure 15. Temperature Profiles for Standard De-Icer Design Studied

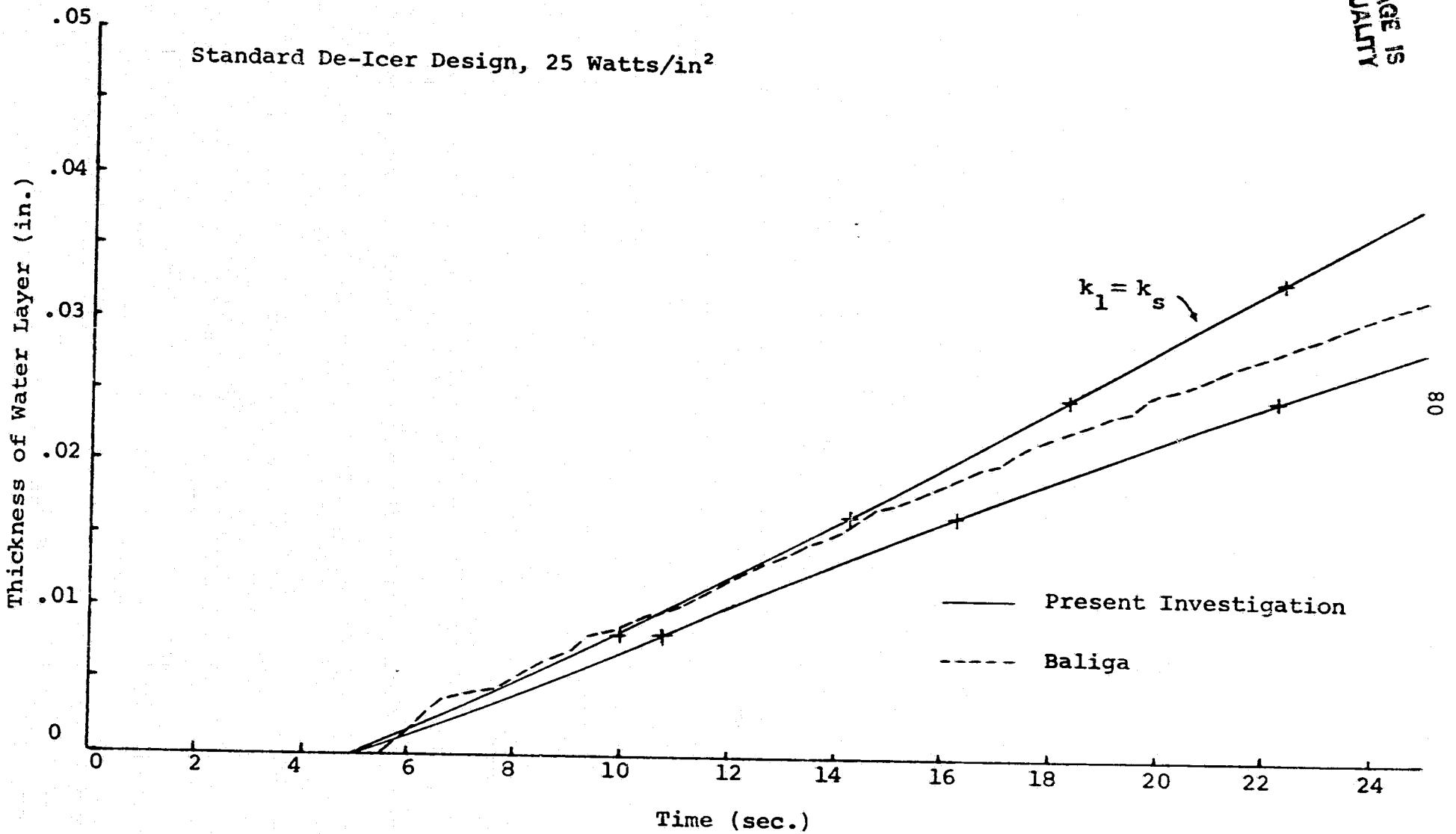

Figure 16. Ice-Water Interface Location

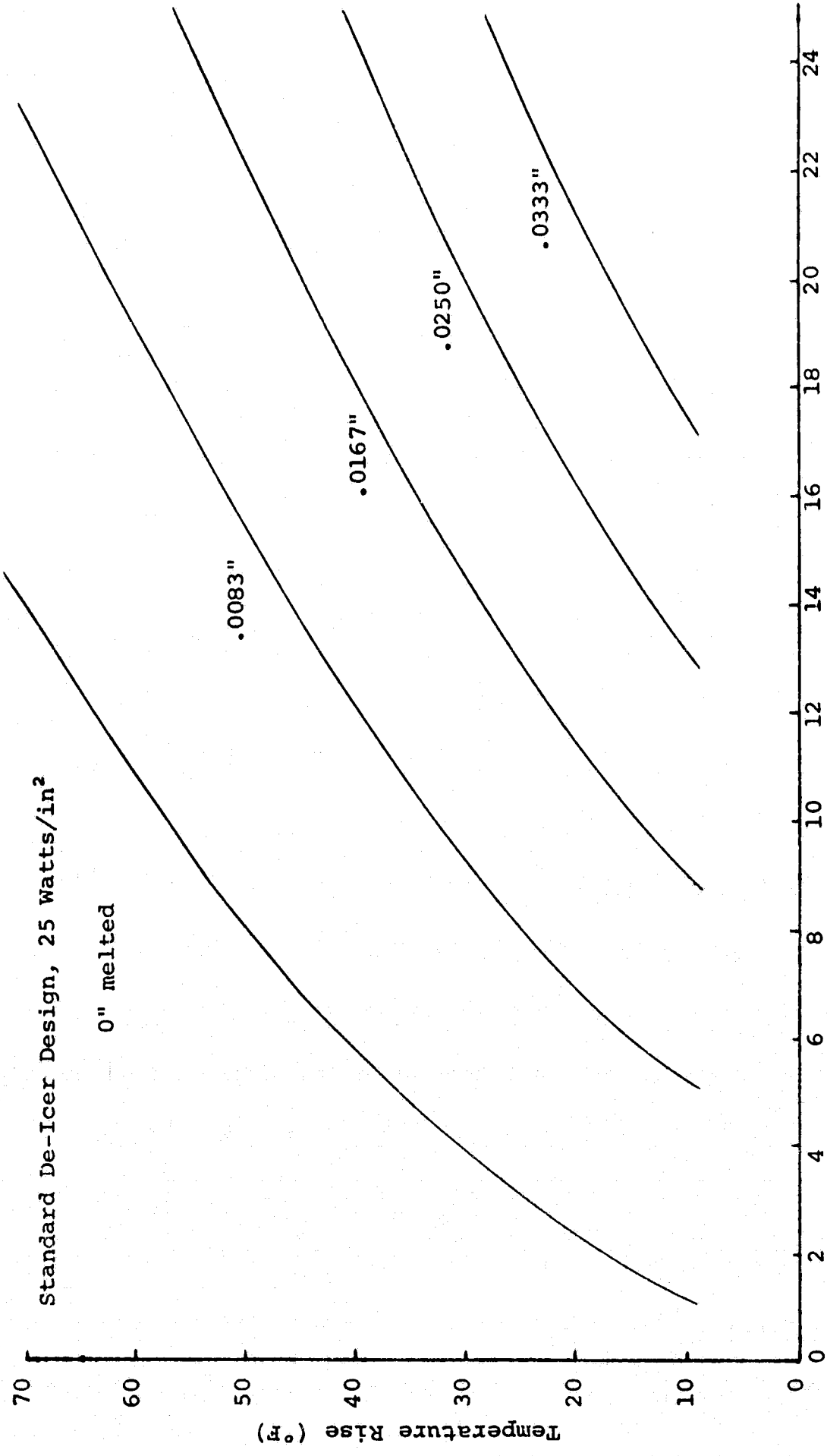

Figure 17. Effect of Ice Layer Thickness Melted on De-Icer Performance

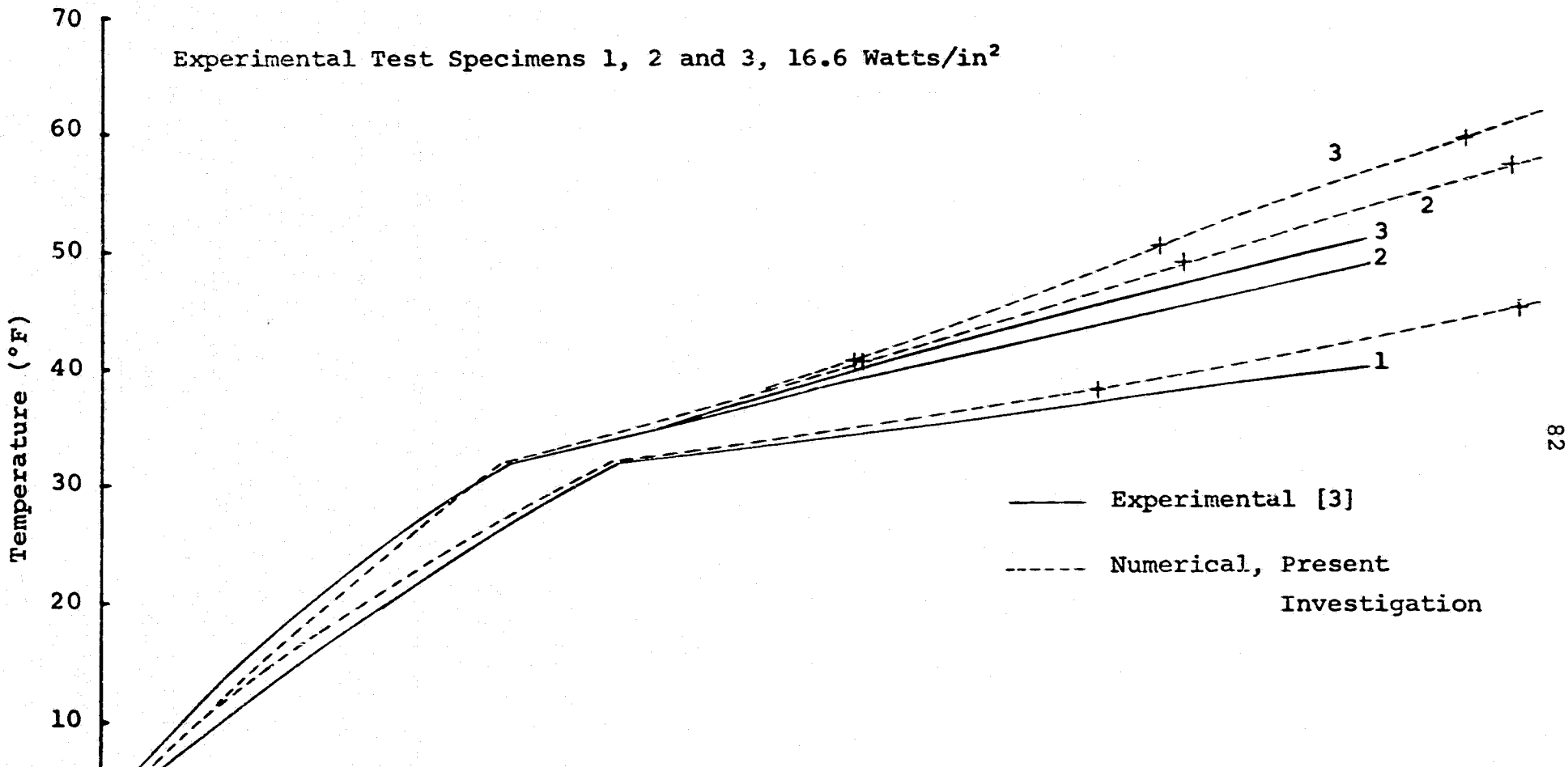

Figure 18. Comparison of Experimental and Predicted Abrasion Shield Temperatures

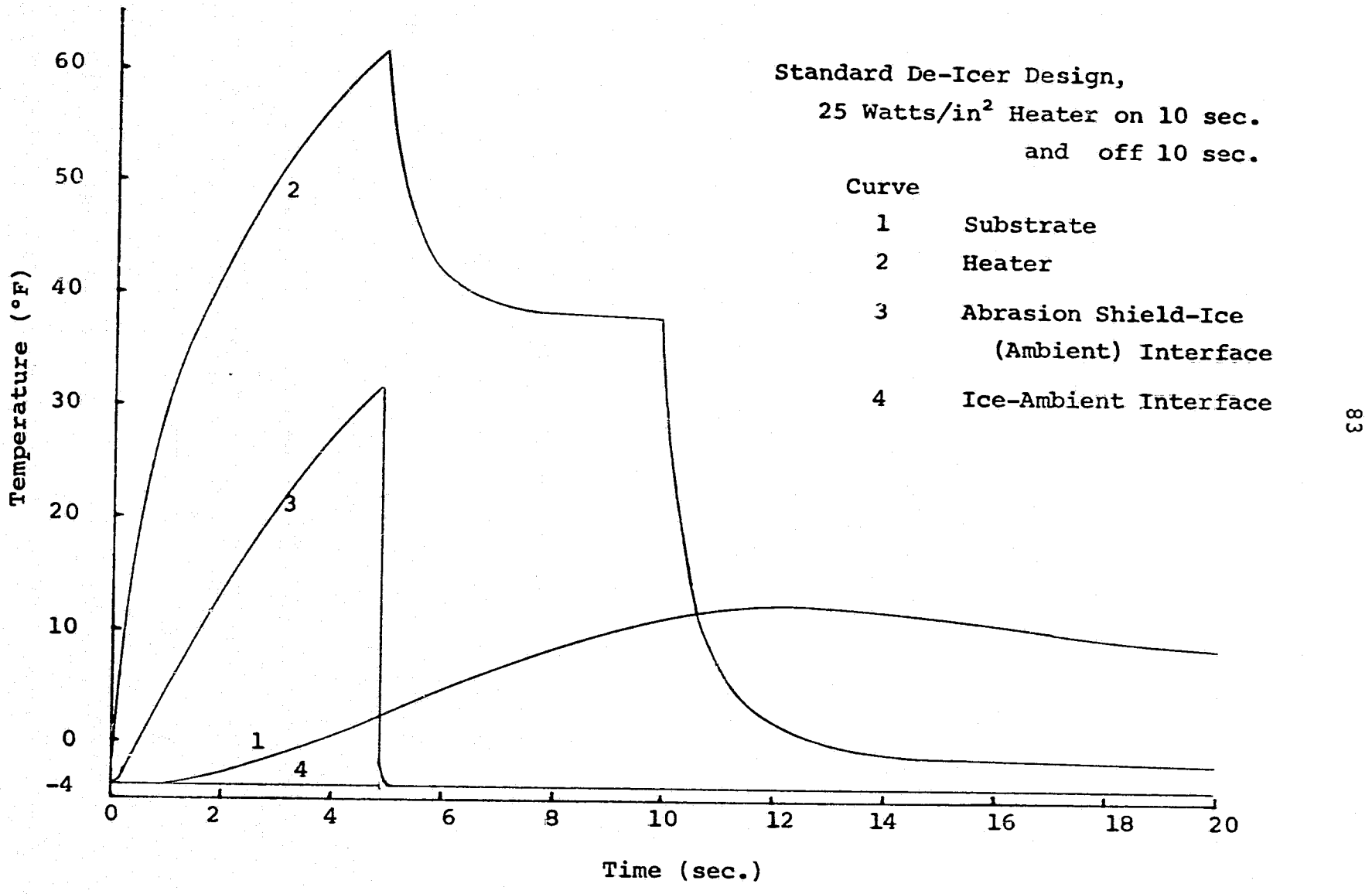

Figure 19. Temperature Response when Ice Layer is Shed, 1st Cycle

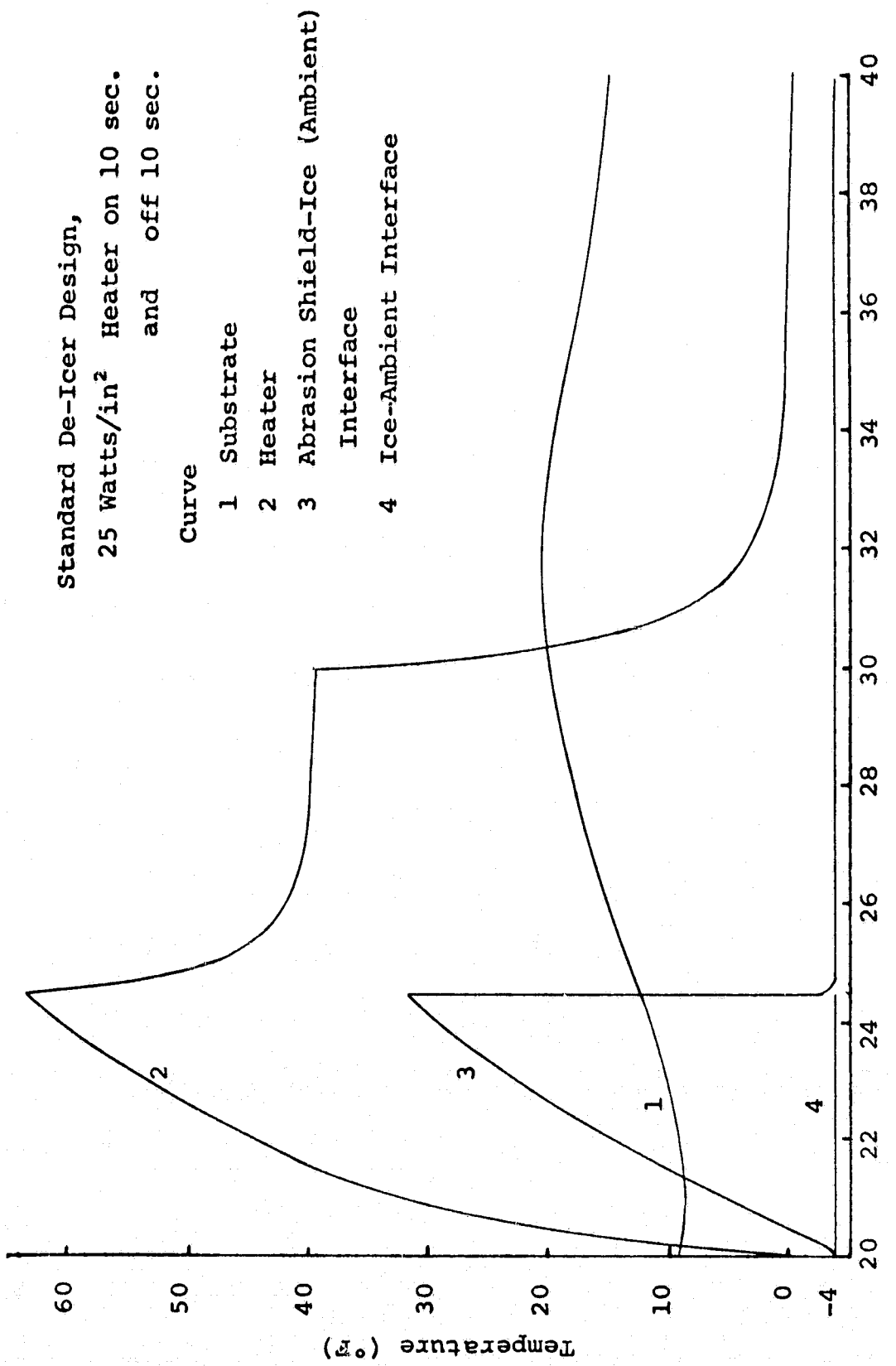

Figure 20. Temperature Response when Ice Layer is Shed, 2nd Cylce

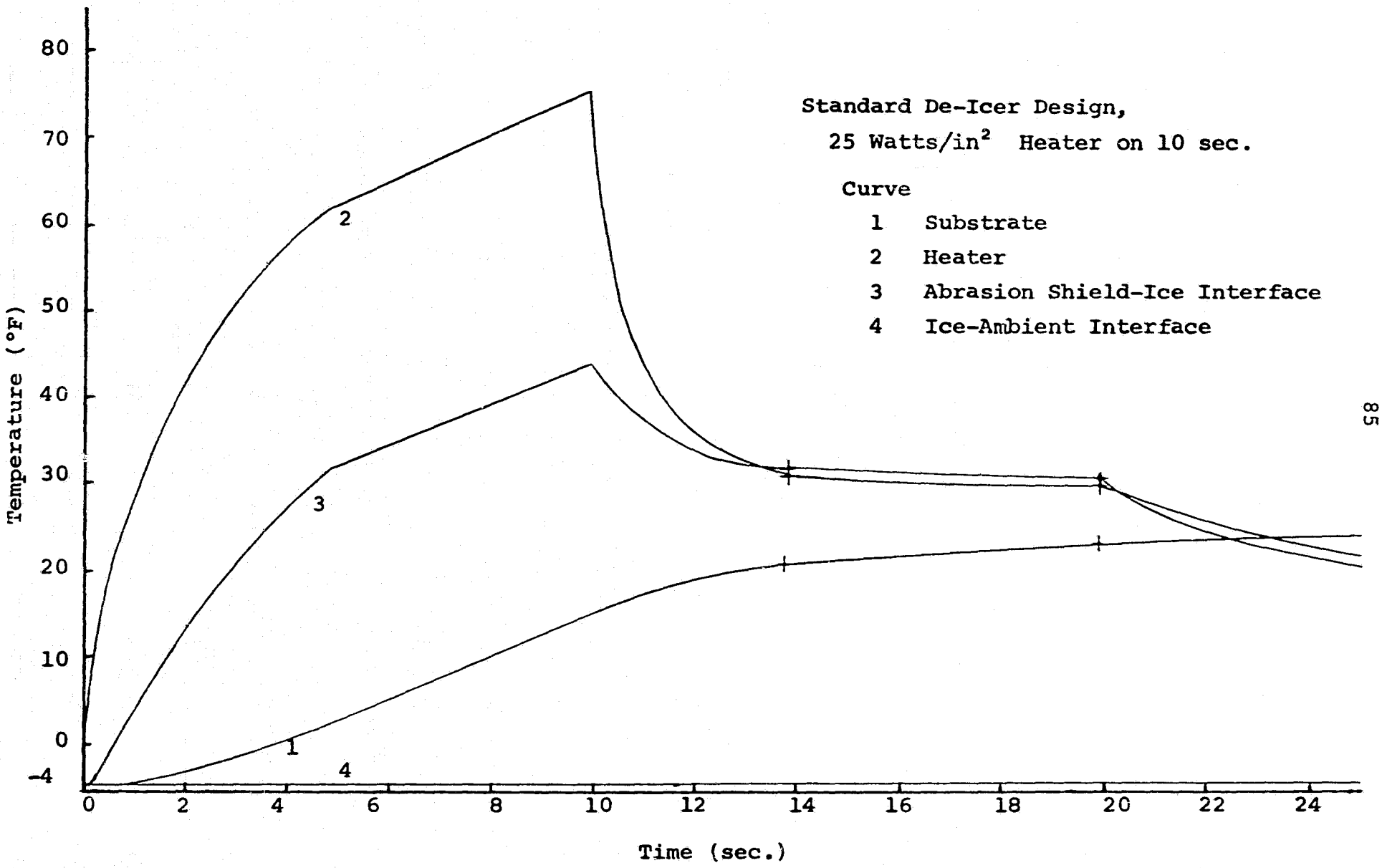

Figure 21. Temperature Response without Ice Shedding

APPENDIX

Complete Program Listing

and

Sample Input Data File

```
//UOFT1275 JOB (UT,
// 06200016,1)
// EXEC FORTXCLG
//FORT.SYSIN  DD *
C
C  HEAT TRANSFER IN A COMPOSITE BODY
C
C  INPUT VARIABLES:
C
C     II, NUMBER OF LAYERS IN BODY, OR ONE LESS IF ICE-WATER LAYER IS
C         INCLUDED.
C     P1=0, NO HEATER; =1, VARIABLE WATTAGE HEATER; =2, CONSTANT
C           WATTAGE HEATER.
C     P2=0, POINT HEATER; =1, FINITE THICKNESS HEATER.
C     P3=1, FINITE THICKNESS HEATER; =2, POINT HEATER.
C     P4=0, NONPERIODIC HEATER; =1, PERIODIC (ON-OFF) HEATER.
C     P5=0, PHASE CHANGE NOT CONSIDERED; =1, PHASE CHANGE CONSIDERED.
C     P6=0, CONSTANT TEMPERATURE B.C. AT INNER SURFACE; =1, CONVECTIVE
C           B.C. AT INNER SURFACE.
C     P7=0, CONSTANT TEMPERATURE B.C. AT OUTER SURFACE; =1, CONVECTIVE
C           B.C. AT OUTER SURFACE (P7.NE.0,IF P5=1).
C     P8=0, CONSTANT TIME STEP USED; =1, VARIABLE TIME STEP USED.
C     P9=0, NO PRINTING; =1, PRINT OUTPUT WHEN T(IX,JX) BECOMES .GE.
C           TO TMAX (USED TO PRINT OUTPUT WHEN ICE BEGINS TO MELT);
C           =2, TERMINATE PROGRAM AFTER ICE BEGINS TO MELT.
C     P10=0, NO LINEAR EXTRAPOLATION; =1, LINEAR EXTRAPOLATION IS USED
C            BETWEEN TIME STEPS TO ESTIMATE NEW TEMPERATURES.
C     P11=0, CONSTANT ACCELERATION PARAMETER IS USED; =1, VARIABLE
C            ACCELERATION PARAMETER IS USED FOR OVER-RELAXATION IN THE
C            SINGLE PHASE LAYERS.
C     P12=0, SHEDING OF ICE LAYER IS NOT CONSIDERED; =1, ICE LAYER
C            IS SHED WHEN THE INTERFACE BETWEEN THE SOLID AND LIQ. IS
C            AT NODE JSH (ISM,DTMM AND DTMF SHOULD BE SPECIFIED).
C     P13=0, INITIAL TEMPERATURE CONSTANT; =1, READ IN INITIAL
C            TEMPERATURE DISTRIBUTION FOR COMPOSITE BODY.
C     P14=0, DO NOT STORE FINAL TEMPERATURES; =1, STORE FINAL
C            TEMPERATURE DISTRIBUTION (P13 AND P14 ARE USED FOR
C            ICE SHEDING PROBLEMS).
C     JJ(I=1,II), NUMBER OF NODES IN LAYER.
C     L(I=1,II), THICKNESS OF LAYER (IN).
C     K(I=1,II), THERMAL CONDUCTIVITY OF LAYER (BTU/HR-FT-'F).
C     DIF(I=1,II), THERMAL DIFFUSIVITY OF LAYER (FT-FT/HR).
C     PI(I=1,II-1)=0, PERFECT CONTACT BETWEEN LAYERS I AND I+1; =1,
C                     CONTACT RESISTANCE BETWEEN LAYERS I AND I+1.
```

```
C     HI(I=1,II-1), HEAT TRANSFER COEFFICIENT BETWEEN LAYERS I AND
C                   I+1 (BTU/HR-FT-FT-'F).
C     IQ, IF P2.EQ.0, HEATER IS LOCATED BETWEEN LAYERS IQ AND IQ+1
C         (IQ.GE.1 AND .LT.II); IF P2.EQ.1, HEATER IS LOCATED IN
C         LAYER IQ (IQ.GT.1 AND .LT.II).
C     C1,C2,C3,A4,A5, CONSTANTS IN THE EQUATION:
C                     QF=C1*TM+C2+C3*COS(A4*TM+A5) WHERE QF IS THE
C                     TOTAL WATTAGE OF THE HEATER (WATTS/IN-IN) AND
C                     TM IS TIME (SEC).
C     TMO, LENGTH OF TIME THE (PERIODIC) HEATER IS ON (SEC).
C     TMF, LENGTH OF TIME THE (PERIODIC) HEATER IS OFF (SEC).
C     TIN, INITIAL TEMPERATURE OF BODY ('F).
C     TA1, AMBIENT TEMPERATURE AT INNER SURFACE ('F).
C     TA2, AMBIENT TEMPERATURE AT OUTER SURFACE ('F).
C     H1, HEAT TRANSFER COEFFICIENT AT INNER SURFACE (BTU/HR-FT-FT-'F).
C     H2, HEAT TRANSFER COEFFICIENT AT OUTER SURFACE (BTU/HR-FT-FT-'F).
C     ISI,ISM, SEE BELOW.
C     DTMI, INITIAL TIME STEP (SEC).
C     DTMM, INTERMEDIATE TIME STEP, USED FOR TIME STEPS .GT.ISI AND
C           .LE.ISM (SEC).
C     DTMF, FINAL TIME STEP, USED FOR TIME STEPS .GT.ISM (SEC).
C     ISF, TOTAL NUMBER OF TIME STEPS.
C     IFRQ, FREQUENCY OF PRINTOUTS.
C     CMAX, CONVERGENCE CRITERIA FOR ITERATION OF TEMPERATURES (%).
C     IWI,IWM, SEE BELOW.
C     WI, INITIAL ACCELERATION PARAMETER FOR OVER-RELAXATION.
C     WM, INTERMEDIATE ACCELERATION PARAMETER, USED FOR TIME STEPS
C         .GT.IWI AND .LE.IWM.
C     WF, FINAL ACCELERATION PARAMETER, USED FOR TIME STEPS .GT.IWM.
C     IX,JX,TMAX, SEE DESCRIPTION OF P9.
C     CF1, CONVERSION FACTOR FROM (IN-IN/SEC) TO (FT-FT/HR).
C     CF2, CONVERSION FACTOR FROM (1/IN) TO (1/FT).
C     CF3, CONVERSION FACTOR FROM (WATTS/IN) TO (BTU/HR-FT).
C     CPS, SPECIFIC HEAT OF ICE (BTU/LB-'F).
C     KS, THERMAT CONDUCTIVITY OF ICE (BTU/HR-FT-'F).
C     DENS, DENSITY OF ICE (LB/FT-FT-FT).
C     MP, MELTING POINT OF WATER ('F).
C     DH, LATENT HEAT OF FUSION (BTU/LB).
C     CPL, SPECIFIC HEAT OF LIQ. WATER (BTU/LB-'F).
C     KL, THERMAL CONDUCTIVITY OF LIQ. WATER (BTU/HR-FT-'F).
C     DENL, DENSITY OF LIQ. WATER (LB/FT-FT-FT).
C     JW, NUMBER OF NODES IN ICE-WATER LAYER.
C     LW, THICKNESS OF ICE-WATER LAYER (IN).
C     JSH, SEE DESCRIPTION OF P12.
C
```

```
      IMPLICIT REAL(K-N)
      INTEGER P1,P4,P5,P6,P7,P8,P9,P10,P11,P12,P13,P14,PI,GS,TERM
      DIMENSION JJ(9),JN(9),L(9),DIF(9),K(9),DX(9),M(9),S(9),N(9)
      DIMENSION PI(9),HI(9),N1(9),N2(9)
      DIMENSION T(70),TO(70)
      DIMENSION TW(91),TWO(91),H(91),HO(91)
      COMMON /AREA1/MP,HSMP,HLMP,HMP,CS,CL,TMP,KS,KL
      COMMON /AREA2/JW,MW,NW,NA2W
      COMMON /AREA5/ISI,ISM,DTMM,DTMF
      COMMON /AREA6/P3,P4,CF3,TMO,PER,AA,A1,A2,A3,A4,A5
      DATA INS/56/,IN/5/,IO/6/,IOS/56/,CF1/25./,CF2/12./
      CF3=40.9463
C
C   INPUT DATA FOR THE COMPOSITE BODY
C
      READ(IN,10)II,P1,P2,P3,P4,P5,P6,P7
      READ(IN,17)P8,P9,P10,P11,P12,P13,P14
      READ(IN,11)(JJ(I),I=1,II)
      READ(IN,12)(L(I),I=1,II)
      READ(IN,12)(K(I),I=1,II)
      READ(IN,12)(DIF(I),I=1,II)
      III=II-1
      READ(IN,11)(PI(I),I=1,III)
      READ(IN,12)(HI(I),I=1,III)
      READ(IN,13)IQ,C1,C2,C3,A4,A5
      READ(IN,14)TMO,TMF
      READ(IN,15)TIN,TA1,TA2,H1,H2
      READ(IN,16)ISI,ISM,DTMI,DTMM,DTMF
      READ(IN,16)ISF,IFRQ,CMAX
      READ(IN,16)IWI,IWM,WI,WM,WF
      READ(IN,16)IX,JX,TMAX
C
C   INITIALIZATION AND CALCULATION OF TIME-INDEPENDENT CONSTANTS
C
      TM=0.
      IS=0
      IP5=P5
      DTM=DTMI
      W=WI
      AA=0.
      PER=TMO+TMF
      TL=0.
      TERM=0
      AGS=0.
      GS=0
```

```
      JN(1)=JJ(1)
      DO 120 I=1,II
      TL=TL+L(I)
      DX(I)=L(I)/(JJ(I)-1)
      M(I)=CF1*DX(I)**2/(DIF(I)*DTM)
      S(I)=0.
      IF(I.EQ.1)GO TO 120
      JN(I)=JN(I-1)+JJ(I)
      IF(PI(I-1).NE.0)GO TO 116
      N(I-1)=K(I)*DX(I-1)/(K(I-1)*DX(I))
      GO TO 120
  116 N1(I-1)=HI(I-1)*DX(I-1)/(K(I-1)*CF2)
      N2(I-1)=HI(I-1)*DX(I)/(K(I)*CF2)
  120 CONTINUE
      IF(P9.EQ.0)GO TO 122
      JXX=JX
      IF(IX.NE.1) JXX=JXX+JN(IX-1)
  122 IF(P13.EQ.0)GO TO 124
C
C   INPUT INITIAL TEMPERATURE DISTRIBUTION FOR COMPOSITE BODY
C
      JN0=1
      DO 123 I=1,200
      JN1=JN0+5
      IF(JN1.GT.JN(II)) JN1=JN(II)
      READ(INS,18)(T(J),J=JN0,JN1)
      IF(JN1.EQ.JN(II)) GO TO 127
      JN0=JN1+1
  123 CONTINUE
  124 JN1=JN(II)
      DO 125 J=1,JN1
      T(J)=TIN
  125 CONTINUE
  127 IF(P6.EQ.0)GO TO 128
      NA1=H1*DX(1)/(K(1)*CF2)
      GO TO 130
  128 T(1)=TA1
  130 IF(P7.EQ.0)GO TO 132
      NA2=H2*DX(II)/(K(II)*CF2)
      GO TO 135
  132 IF(P5.EQ.0) T(JN(II))=TA2
  135 IF(P1.EQ.0)GO TO 140
      IF(P2.EQ.0.)GO TO 138
      A1=C1*DX(IQ)/L(IQ)
      A2=C2*DX(IQ)/L(IQ)
```

```
      A3=C3*DX(IQ)/L(IQ)
      GO TO 140
  138 A1=C1
      A2=C2
      A3=C3
C
C  PRINT DATA FOR THE COMPOSITE BODY
C
  140 WRITE(IO,20)
      WRITE(IO,21)
      WRITE(IO,22)
      IF(P5.EQ.0)GO TO 145
      IPRT=II+1
      WRITE(IO,23)IPRT
      WRITE(IO,24)
      GO TO 150
  145 WRITE(IO,23)II
      WRITE(IO,25)
  150 WRITE(IO,26)
      WRITE(IO,27)
      WRITE(IO,28)
      WRITE(IO,29)
      WRITE(IO,30)
      DO 160 I=1,II
      WRITE(IO,31)I,JJ(I),L(I),DX(I),K(I),DIF(I)
  160 CONTINUE
      WRITE(IO,32)TL
      IF(P1.EQ.0)GO TO 200
      WRITE(IO,33)
      WRITE(IO,34)
      IF(P2.EQ.1.)GO TO 170
      IQ1=IQ+1
      WRITE(IO,35)IQ,IQ1
      GO TO 180
  170 WRITE(IO,36)IQ
  180 IF(P4.EQ.0)GO TO 190
      WRITE(IO,37)TMO
      WRITE(IO,39)TMF
  190 WRITE(IO,40)
      WRITE(IO,41)
      WRITE(IO,42)C1,C2,C3
      WRITE(IO,43)A4,A5
  200 WRITE(IO,44)
      WRITE(IO,45)
      WRITE(IO,46)TIN
```

```
      IF(P6.NE.0)GO TO 210
      WRITE(IO,47)TA1
      GO TO 220
  210 WRITE(IO,48)
      WRITE(IO,49)TA1
      WRITE(IO,50)H1
  220 IF(P7.NE.0)GO TO 230
      WRITE(IO,51)TA2
      GO TO 240
  230 WRITE(IO,52)
      WRITE(IO,49)TA2
      WRITE(IO,50)H2
  240 DO 241 I=1,III
      IF(PI(I).EQ.0)GO TO 241
      IPRT=I+1
      WRITE(IO,87)I,IPRT
      WRITE(IO,50)HI(I)
  241 CONTINUE
C
C   INPUT DATA FOR ICE-WATER LAYER IF INCLUDED
C
      IF(P5.EQ.0)GO TO 260
      READ(IN,14)CPS,KS,DENS,MP,DH
      READ(IN,14)CPL,KL,DENL
      READ(IN,16)JW,JSH,LW
C
C   INITIALIZATION AND CALCULATION OF TIME-INDEPENDENT CONSTANTS
C
      HSMP=DENS*CPS*MP
      HLMP=DENL*(CPS*MP+DH)
      HMP=.5*(HLMP+HSMP)
      CS=DENS*CPS
      CL=DENL*CPL
      TMP=MP-HLMP/CL
      IF(TIN.LE.MP) HIN=CS*TIN
      IF(TIN.GT.MP) HIN=CL*(TIN-TMP)
      DO 247 J=1,JW
      TW(J)=TIN
      H(J)=HIN
  247 CONTINUE
      DXW=LW/(JW-1)
      MW=DTM/(DXW**2*CF1)
      NW=K(II)*DXW/DX(II)
      NA2W=H2*DXW/CF2
C
```

```
C   PRINT DATA FOR THE ICE-WATER LAYER
C
      WRITE(IO,53)
      WRITE(IO,54)
      WRITE(IO,55)
      WRITE(IO,56)DENS,DENL
      WRITE(IO,57)CPS,CPL
      WRITE(IO,58)KS,KL
      WRITE(IO,59)HSMP,HLMP
      WRITE(IO,60)MP
      WRITE(IO,61)DH
      WRITE(IO,62)TIN
      WRITE(IO,63)HIN
      WRITE(IO,64)LW
      WRITE(IO,65)JW,DXW
      IF(P12.EQ.0)GO TO 260
      WRITE(IO,96)JSH
  260 WRITE(IO,66)
      WRITE(IO,67)
      WRITE(IO,95)IN
      IF(P8.EQ.0)GO TO 270
      WRITE(IO,68)
      WRITE(IO,69)DTMI,ISI
      ISI1=ISI+1
      WRITE(IO,70)DTMM,ISI1,ISM
      ISM1=ISM+1
      WRITE(IO,71)DTMF,ISM1
      GO TO 280
  270 WRITE(IO,72)DTMI
  280 WRITE(IO,73)IFRQ
      WRITE(IO,74)CMAX
      IF(P10.EQ.0)GO TO 282
      WRITE(IO,86)
  282 IF(P11.EQ.0)GO TO 284
      WRITE(IO,90)
      WRITE(IO,91)WI,IWI
      IWI1=IWI+1
      WRITE(IO,92)WM,IWI1,IWM
      IWM1=IWM+1
      WRITE(IO,93)WF,IWM1
      GO TO 286
  284 WRITE(IO,94)WI
  286 WRITE(IO,75)
      WRITE(IO,76)
      WRITE(IO,77)
```

```
      IF(P13.EQ.0)GO TO 290
      WRITE(IO,78)TM,GS
      JN0=1
      DO 287 I=1,II
      WRITE(IO,79)I
      JN1=JN(I)
      WRITE(IO,80)(T(J),J=JN0,JN1)
      JN0=JN1+1
  287 CONTINUE
      IF(P5.EQ.0)GO TO 290
      IPRT=II+1
      WRITE(IO,81)IPRT
      WRITE(IO,80)(TW(J),J=1,JW)
      WRITE(IO,82)
      WRITE(IO,89)(H(J),J=1,JW)
C
C  INITIALIZATION OF VARIABLES FOR NEW TIME STEP
C
  290 IS=IS+1
      P5=IP5
      JN1=JN(II)
      DO 300 J=1,JN1
      IF(P10.EQ.0.OR.IS.EQ.1)GO TO 292
C
C  LINEAR EXTRAPOLATION
C
      TEXT=2.*T(J)-TO(J)
  292 TO(J)=T(J)
      IF(P10.EQ.0.OR.IS.EQ.1)GO TO 300
      T(J)=TEXT
  300 CONTINUE
      IF(P5.EQ.0)GO TO 320
      DO 310 J=1,JW
      IF(P10.EQ.0.OR.IS.EQ.1)GO TO 302
C
C  LINEAR EXTRAPOLATION
C
      HEXT=2.*H(J)-HO(J)
  302 HO(J)=H(J)
      TWO(J)=TW(J)
      IF(P10.EQ.0.OR.IS.EQ.1)GO TO 310
      H(J)=HEXT
      IF(H(J).LE.HSMP) JP=1
      IF(H(J).GT.HSMP.AND.H(J).LT.HLMP) JP=2
      IF(H(J).GE.HLMP) JP=3
```

```
      GO TO(304,305,306),JP
  304 TW(J)=H(J)/CS
      GO TO 310
  305 TW(J)=MP
      GO TO 310
  306 TW(J)=H(J)/CL+TMP
  310 CONTINUE
  320 IF(P8.EQ.0)GO TO 330
C
C   ADJUSTMENT OF CONSTANTS IF TIME STEP CHANGES
C
      CALL STEP(P5,II,IS,DTM,M,MW)
  330 IF(P11.EQ.0)GO TO 332
C
C   ADJUSTMENT OF ACCELERATION PARAMETER
C
      IF(IS.EQ.IWI+1) W=WM
      IF(IS.EQ.IWM+1) W=WF
  332 IF(P1.EQ.0)GO TO 340
      IF(P1.EQ.2.AND.IS.GT.1)GO TO 340
C
C   CALCULATION OF NEW SOURCE TERM
C
      CALL SOURCE(DX(IQ),K(IQ),S(IQ),TM,DTM)
C
C   CALCULATION OF NEW TIME
C
  340 TM=TM+DTM
C
C   GAUSS-SEIDEL REITERATION
C
      DO 400 GS=1,200
      ICV=0
      IF(P6.EQ.0)GO TO 350
C
C   CALCULATION OF TEMPERATURE AT THE INNER-AMBIENT INTERFACE
C
      TOLD=T(1)
      T(1)=T(1)+W*((T(2)+TO(2)-((1.-M(1))+NA1)*TO(1)
     1+2.*NA1*TA1)/(1.+M(1)+NA1)-T(1))
      CALL CONVE(TOLD,T(1),CMAX,ICV)
  350 JN0=2
      DO 360 I=1,II
      JN1=JN(I)-1
      IF(JN1.LT.JN0)GO TO 356
```

```
      DO 355 J=JN0,JN1
C
C  CALCULATION OF TEMPERATURES IN THE INTERIOR OF THE LAYER
C
      TOLD=T(J)
      T(J)=T(J)+W*((T(J+1)+T(J-1)+TO(J+1)+2.*(M(I)-1.)*TO(J)
     1+TO(J-1)+2.*P2*S(I))/(2.*(M(I)+1.))-T(J))
      IF(ICV.NE.0)GO TO 355
      CALL CONVE(TOLD,T(J),CMAX,ICV)
  355 CONTINUE
  356 IF(I.EQ.II)GO TO 370
      IF(PI(I).NE.0)GO TO 357
C
C  CALCULATION OF TEMPERATURE AT THE INTERFACE BETWEEN LAYERS,
C  NON-RESISTIVE INTERFACE
C
      TOLD=T(JN1+1)
      T(JN1+1)=T(JN1+1)-W*(T(JN1+1)-(T(JN1)+N(I)*T(JN1+3)+TO(JN1)
     1+((M(I)-1.)+N(I)*(M(I+1)-1.))*TO(JN1+1)+N(I)*TO(JN1+3)
     1+S(I)+P2*N(I)*S(I+1))/(1.+M(I)+N(I)*(1.+M(I+1))))
      T(JN1+2)=T(JN1+1)
      IF(ICV.NE.0)GO TO 359
      CALL CONVE(TOLD,T(JN1+1),CMAX,ICV)
      GO TO 359
C
C  CALCULATION OF TEMPERATURES AT THE INTERFACE BETWEEN LAYERS,
C  RESISTIVE INTERFACE
C
  357 TOLD=T(JN1+1)
      T(JN1+1)=T(JN1+1)+W*((T(JN1)+N1(I)*(T(JN1+2)+TO(JN1+2))-
     1(1.-M(I)+N1(I))*TO(JN1+1)+TO(JN1)+S(I))/(1.+M(I)+N1(I))-T(JN1+1))
      IF(ICV.NE.0)GO TO 358
      CALL CONVE(TOLD,T(JN1+1),CMAX,ICV)
  358 TOLD=T(JN1+2)
      T(JN1+2)=T(JN1+2)+W*((T(JN1+3)+N2(I)*(T(JN1+1)+TO(JN1+1))-
     1(1.-M(I+1)+N2(I))*TO(JN1+2)+TO(JN1+3)+P2*S(I+1))/
     1(1.+M(I+1)+N2(I))-T(JN1+2))
      IF(ICV.NE.0)GO TO 359
      CALL CONVE(TOLD,T(JN1+2),CMAX,ICV)
  359 JN0=JN1+3
  360 CONTINUE
  370 IF(P5.NE.0)GO TO 385
      IF(P7.EQ.0)GO TO 390
C
C  CALCULATION OF TEMPERATURE AT THE OUTER-AMBIENT INTERFACE
```

```
C
      TOLD=T(JN1+1)
      T(JN1+1)=T(JN1+1)+W*((T(JN1)+TO(JN1)-((1.-M(II))+NA2)
     1*TO(JN1+1)+2.*NA2*TA2)/(1.+M(II)+NA2)-T(JN1+1))
      IF(ICV.NE.0)GO TO 390
      CALL CONVE(TOLD,T(JN1+1),CMAX,ICV)
      GO TO 390
C
C  CALCULATION OF TEMPERATURES IN THE ICE-WATER LAYER
C  IF INCLUDED
C
  385 CALL WLAYER(TW,TWO,H,HO,T(JN1),TO(JN1),T(JN1+1),TA2,
     1M(II),CMAX,ICV,GS)
C
C  CHECK CONVERGENCE OF THE GAUSS-SEIDEL ITERATION
C
  390 IF(ICV.EQ.0)GO TO 410
  400 CONTINUE
  410 WRITE(IO,78)TM,GS
      AGS=AGS+FLOAT(GS)
C
C  DETERMINATION OF WHETHER ICE LAYER SHOULD BE SHED
C
      IF(P5.EQ.0.OR.P12.EQ.0)GO TO 415
      HJSH=H(JSH)
      IF(JSH.EQ.1) HJSH=HMP+.5*(H(JSH)-HSMP)
      IF(HJSH.LT.HMP)GO TO 415
      IP5=0
      P8=1
      ISI=IS
C
C  DETERMINATION OF WHETHER THE PROGRAM SHOULD BE TERMINATED
C
  415 IF(IS.EQ.ISF)TERM=1
C
C  DETERMINATION OF WHETHER OUTPUT SHOULD BE PRINTED
C
      IF(P5.NE.IP5)GO TO 430
      IF(P9.EQ.0)GO TO 420
      IF(TO(JXX).LT.TMAX.AND.T(JXX).GE.TMAX)GO TO 429
  420 IF(IS/IFRQ*IFRQ.EQ.IS.OR.TERM.NE.0)GO TO 430
      GO TO 290
C
C  PRINT OUTPUT OF PROGRAM
C
```

```
  429 IF(P9.EQ.2) TERM=1
  430 JN0=1
      DO 440 I=1,II
      WRITE(IO,79)I
      JN1=JN(I)
      WRITE(IO,80)(T(J),J=JN0,JN1)
      JN0=JN1+1
  440 CONTINUE
      IF(P5.EQ.0)GO TO 455
      IPRT=II+1
      WRITE(IO,81)IPRT
      WRITE(IO,80)(TW(J),J=1,JW)
      WRITE(IO,82)
      WRITE(IO,89)(H(J),J=1,JW)
  455 IF(TERM.NE.0)GO TO 460
      GO TO 290
C
C   STORE TEMPERATURE DATA FOR NEXT RUN
C
  460 IF(P14.EQ.0)GO TO 465
      JN0=1
      DO 462 I=1,200
      JN1=JN0+5
      IF(JN1.GT.JN(II)) JN1=JN(II)
      WRITE(IOS,18)(T(J),J=JN0,JN1)
      IF(JN1.EQ.JN(II))GO TO 465
      JN0=JN1+1
  462 CONTINUE
C
C   PRINT REASON WHY PROGRAM WAS TERMINATED
C
  465 WRITE(IO,85)IS
      AVER=AGS/FLOAT(IS)
      WRITE(IO,88)AVER
      STOP
C
C   FORMAT STATEMENTS FOR INPUT AND OUTPUT
C
   10 FORMAT(3X,I2,5X,I1,5X,F1.0,5X,F1.0,5X,I1,5X,I1,5X,I1,5X,I1)
   11 FORMAT(5X,8I8)
   12 FORMAT(5X,8F8.0)
   13 FORMAT(5X,I6,5X,F6.0,5X,F6.0,5X,F6.0,5X,F6.0,5X,F6.0,5X,F6.0)
   14 FORMAT(5X,F6.0,5X,F6.0,5X,F6.0,5X,F6.0,5X,F6.0,5X,F6.0,5X,F6.0)
   15 FORMAT(5X,F6.0,5X,F6.0,5X,F6.0,5X,F6.0,5X,F8.0,5X,F8.0)
   16 FORMAT(5X,I6,5X,I6,5X,F6.0,5X,F6.0,5X,F6.0,5X,F6.0)
```


ORIGINAL PAGE IS
OF POOR QUALITY

```
17 FORMAT(10X,I1,5X,I1,5X,I1,5X,I1,5X,I1,5X,I1,5X,I1)
18 FORMAT(6F12.5)
20 FORMAT(19X,'-----------------------------------------')
21 FORMAT(19X,'HEAT TRANSFER ANALYSIS OF A COMPOSITE BODY')
22 FORMAT(19X,'-----------------------------------------')
23 FORMAT(//,5X,'THERE ARE',I2,X,'LAYERS IN THE BODY.')
24 FORMAT(/,5X,'THE PHASE CHANGE IN THE ICE-WATER LAYER
  1 IS CONSIDERED.')
25 FORMAT(/,5X,'A PHASE CHANGE IS NOT CONSIDERED.')
26 FORMAT(//,5X,'PHYSICAL PROPERTY DATA FOR LAYERS')
27 FORMAT(5X,'-------------------------------')
28 FORMAT(/,5X,'LAYER',4X,'NUMBER',5X,'LENGTH',6X,'DELTA X',6X,
  1'THERMAL',7X,'THERMAL')
29 FORMAT(5X,'NUMBER',2X,'OF NODES',26X,'CONDUCTIVITY',3X,
  1'DIFFUSIVITY')
30 FORMAT(26X,'(IN)',8X,'(IN)',4X,'(BTU/HR-FT-''F)',2X,'(FT-FT/HR)'
  1)
31 FORMAT(/,6X,I2,8X,I2,6X,F7.4,6X,F7.5,6X,F6.3,8X,F6.4)
32 FORMAT(/,9X,'TOTAL LENGTH = ',F7.4)
33 FORMAT(//,5X,'DATA FOR HEATER')
34 FORMAT(5X,'---------------')
35 FORMAT(/,5X,'THE HEATER IS A POINT HEAT SOURCE LOCATED
  1 BETWEEN LAYERS',I2,X,'AND',I2,'.')
36 FORMAT(/,5X,'THE HEATER HAS A FINITE THICKNESS, AND IS
  1 LOCATED IN LAYER',I2,'.')
37 FORMAT(/,5X,'THE HEATER IS ON PERIODICALLY:',10X,'TIME ON  = ',
  1F6.3,X,'(SEC)')
39 FORMAT(/,45X,'TIME OFF = ',F6.3,X,'(SEC)')
40 FORMAT(/,5X,'THE TOTAL HEAT GENERATION IS GIVEN BY:')
41 FORMAT(/,13X,'QF = C1*TM + C2 + C3*COS(C4*TM + C5)',5X,'(WATTS/
  1IN-IN)')
42 FORMAT(/,13X,'C1 = ',F7.3,10X,'C2 = ',F7.3,10X,'C3 = ',F7.3)
43 FORMAT(/,13X,'C4 = ',F7.3,10X,'C5 = ',F7.3)
44 FORMAT(//,5X,'INITIAL AND BOUNDARY CONDITIONS')
45 FORMAT(5X,'-----------------------------')
46 FORMAT(/,5X,'INITIAL TEMPERATURE IN THE COMPOSITE BODY = ',
  1F6.2,X,'(''F)')
47 FORMAT(/,5X,'CONSTANT TEMPERATURE AT THE INNER-AMBIENT
  1 INTERFACE = ',F6.2,X,'(''F)')
48 FORMAT(/,5X,'CONVECTIVE BOUNDARY CONDITIONS AT THE INNER-
  1AMBIENT INTERFACE:')
49 FORMAT(/,19X,'AMBIENT TEMPERATURE = ',F6.2,X,'(''F)')
50 FORMAT(/,13X,'HEAT TRANSFER COEFFICIENT = ',F10.2,X,
  1'(BTU/HR-FT-FT-''F)')
51 FORMAT(/,5X,'CONSTANT TEMPERATURE AT THE OUTER-AMBIENT
```

```
  1 INTERFACE = ',F6.2,X,'(''F)')
52 FORMAT(/,5X,'CONVECTIVE BOUNDARY CONDITIONS AT THE OUTER-
  1AMBIENT INTERFACE:')
53 FORMAT(//,5X,'PROPERTY DATA FOR THE ICE-WATER LAYER')
54 FORMAT(5X,'-----------------------------------')
55 FORMAT(/,5X,'PROPERTIES OF WATER:',13X,'ICE',8X,'LIQ.
  1 WATER')
56 FORMAT(/,5X,'DENSITY',18X,'=',4X,F8.4,6X,F8.4,2X,
  1'(LBS/FT-FT-FT)')
57 FORMAT(/,5X,'SPECIFIC HEAT',12X,'=',4X,F8.4,6X,F8.4,2X
  1'(BTU/LB-''F)')
58 FORMAT(/,5X,'THERMAL CONDUCTIVITY',5X,'=',4X,F8.4,6X,F8.4,2X,
  1'(BTU/HR-FT-''F)')
59 FORMAT(/,5X,'ENTHALPY AT MELTING PT.',2X,'=',3X,F9.4,5X,F9.4,2X
  1'(BTU/FT-FT-FT)')
60 FORMAT(/,5X,'MELTING POINT OF WATER',10X,'=',8X,F5.2,X,'(''F)')
61 FORMAT(/,5X,'LATENT HEAT OF FUSION',11X,'=',5X,F8.3,X,'(BTU
  1/LB)')
62 FORMAT(/,5X,'INITIAL TEMPERATURE IN LAYER',4X,'=',7X,F6.2,X,
  1'(''F)')
63 FORMAT(/,5X,'INITIAL ENTHALPY IN LAYER',7X,'=',4X,F9.3,X,
  1'(BTU/FT-FT-FT)')
64 FORMAT(/,5X,'LENGTH OF LAYER',17X,'=',6X,F7.4,X,'(IN)')
65 FORMAT(/,5X,'THERE ARE',I3,X,'NODES AND DELTA X',2X,'=',6X,
  1F7.5,X,'(IN)')
66 FORMAT(//,5X,'ADDITIONAL DATA')
67 FORMAT(5X,'---------------')
68 FORMAT(/,5X,'A VARIABLE TIME STEP IS USED:')
69 FORMAT(/,5X,'INITIAL TIME STEP',6X,'=',X,F4.2,X,'(SEC),',
  1' TIME STEPS   1 THROUGH',I4)
70 FORMAT(/,5X,'INTERMEDIATE TIME STEP =',X,F4.2,X,'(SEC),',
  1' TIME STEPS',I4,X,'THROUGH',I4)
71 FORMAT(/,5X,'FINAL TIME STEP',8X,'=',X,F4.2,X,'(SEC),',
  1' TIME STEPS',I4,X,'ON')
72 FORMAT(/,5X,'CONSTANT TIME STEP =',X,F4.2,X,'(SEC)')
73 FORMAT(/,5X,'OUTPUT IS PRINTED EVERY',I2,X,'TIME STEPS.')
74 FORMAT(/,5X,'THE CONVERGENCE CRITERIA FOR TEMPERATURE
  1 IS ',F6.4,X,'%.')
75 FORMAT(//,24X,'---------------------------------')
76 FORMAT(24X,'TEMPERATURE PROFILES IN DEGREES F')
77 FORMAT(24X,'---------------------------------')
78 FORMAT(//,24X,'TIME =',F8.3,X,'(SEC),',5X,'GS =',I3)
79 FORMAT(/,5X,'LAYER',I2)
80 FORMAT(/,6F12.5)
81 FORMAT(/,5X,'LAYER',I2,':  ICE-WATER LAYER')
```

```
   82 FORMAT(/,5X,'ENTHALPY IN ICE-WATER LAYER, BTU/FT-FT-FT')
   85 FORMAT(//,5X,'THE PROGRAM WAS TERMINATED AFTER',I4,X,'TIME
     1 STEPS WERE COMPLETED.')
   86 FORMAT(/,5X,'LINEAR EXTRAPOLATION IS USED BETWEEN TIME STEPS'//
     17X,'TO INITIALIZE TEMPERATURES.')
   87 FORMAT(/,5X,'INTERFACIAL RESISTANCE BETWEEN LAYERS'
     1,I2,X,'AND',I2,':')
   88 FORMAT(/,5X,'THE AVERAGE NUMBER OF ITERATIONS PER TIME
     1STEP WAS',F6.2,X,'.')
   89 FORMAT(/,6F12.3)
   90 FORMAT(/,5X,'A VARIABLE ACCELERATION PARAMETER IS USED FOR
     1 OVER-RELAXATION:')
   91 FORMAT(/,5X,'INITIAL PARAMETER',6X,'=',X,F4.2,X,',',' TIME
     1 STEPS    1 THROUGH',I4)
   92 FORMAT(/,5X,'INTERMEDIATE PARAMETER =',X,F4.2,X,',',' TIME
     1 STEPS',I4,X,'THROUGH',I4)
   93 FORMAT(/,5X,'FINAL PARAMETER',8X,'=',X,F4.2,X,',',' TIME
     1 STEPS',I4,X,'ON')
   94 FORMAT(/,5X,'THE CONSTANT ACCELERATION PARAMETER FOR
     1 OVER-RELAXATION IS',X,F4.2,X,'.')
   95 FORMAT(/,5X,'INPUT DATA FILE ',I3,X,'.')
   96 FORMAT(/,5X,'LAYER IS SHED WHEN THE ICE-WATER INTERFACE IS
     1 AT NODE',I3,'.')
      END
C
      SUBROUTINE STEP(P5,II,IS,DTM,M,MW)
C
C  STEP DETERMINES NEW TIME STEP AND ADJUSTS TIME-STEP DEPENDENT
C  CONSTANTS
C
      REAL M(6),MW
      COMMON /AREA5/ISI,ISM,DTMM,DTMF
      A=DTM
      IF(IS.EQ.ISI+1) DTM=DTMM
      IF(IS.EQ.ISM+1) DTM=DTMF
      IF(A.EQ.DTM)RETURN
      DO 10 I=1,II
      M(I)=M(I)*A/DTM
   10 CONTINUE
      IF(P5.EQ.0)RETURN
      MW=MW*DTM/A
      RETURN
      END
C
      SUBROUTINE SOURCE(DX,K,S,TM,DTM)
```

```
C
C   SOURCE DETERMINES THE VALUE OF THE SOURCE TERM AT A HALF-TIME STEP
C
      INTEGER P4
      REAL K
      COMMON /AREA6/P3,P4,CF3,TMO,PER,AA,A1,A2,A3,A4,A5
C
C   CALCULATION OF HALF TIME
C
      TMH=TM+.5*DTM
      IF(P4.EQ.0)GO TO 10
      IF(TMH.GT.AA*PER.AND.TMH.LE.(AA+1.)*PER)GO TO 10
      AA=AA+1.
C
C   ADJUSTMENT OF TIME FOR PERIODIC HEATERS
C
   10 TMP=TMH-AA*PER
      IF(P4.EQ.0)GO TO 20
      IF(TMP.LE.TMO)GO TO 20
C
C   HEATER OFF
C
      QF=0.
      GO TO 30
C
C   HEATER ON
C
   20 QF=A1*TMP+A2+A3*COS(A4*TMP+A5)
C
C   CALCULATION OF SOURCE TERM
C
   30 S=P3*CF3*DX*QF/K
      RETURN
      END
C
      SUBROUTINE CONVE(TOLD,T,CMAX,ICV)
C
C   CONVE DETERMINES THE PERCENT DIFFERENCE BETWEEN THE NEW AND OLD
C   TEMPERATURES AT A NODE FOR THE GAUSS-SEIDEL METHOD
C
      DIFF=100.*ABS((T-TOLD)/T)
      IF(DIFF.GE.CMAX) ICV=1
      RETURN
      END
C
```

```
      SUBROUTINE WLAYER(TW,TWO,H,HO,T0,TO0,T1,TA2,M,CMAX,ICV,IGS)
C
C  WLAYER CALCULATES THE TEMPERATURES IN THE ICE-WATER LAYER USING
C  THE METHOD OF WEAK SOLUTION
C
      IMPLICIT REAL(K-N)
      COMMON /AREA1/MP,HSMP,HLMP,HMP,CS,CL,TMP,KS,KL
      COMMON /AREA2/JW,MW,NW,NA2W
      DIMENSION TW(91),TWO(91),H(91),HO(91),CNDO(91)
C
C  CALCULATION OF ENTHALPY AND TEMPERATURE AT THE SHIELD-WATER
C  INTERFACE
C
      TOLD=TW(1)
      IF(IGS.NE.1)GO TO 9
      CALL PHASE(1,HO(1),HO(2),JPO,KO2)
      CNDO(1)=KO2*(TWO(2)-TWO(1))
      KO1=KO2
    9 CALL PHASE(1,H(1),H(2),JP,K2)
      GO TO(10,11,11,12),JP
C  ICE
   10 H(1)=(HO(1)+MW*NW*(T0+TO0+(M-1.)*TWO(1))+MW*(K2*TW(2)
     1+CNDO(1)))/(1.+MW*(NW*(M+1.)+K2)/CS)
      TW(1)=H(1)/CS
      IF(H(1).LE.HSMP)GO TO 15
      JP=1
C  M.P.
   11 H(1)=HO(1)+MW*NW*(T0-(M+1.)*MP+TO0+(M-1.)*TWO(1))
     1+MW*(K2*(TW(2)-MP)+CNDO(1))
      TW(1)=MP
      IF(H(1).GT.HSMP.AND.H(1).LT.HLMP)GO TO 15
      IF(JP.EQ.1.OR.JP.EQ.4)GO TO 15
C  LIQ. WATER
   12 H(1)=(HO(1)+MW*NW*(T0-(M+1.)*TMP+TO0+(M-1.)*TWO(1))
     1+MW*(K2*(TW(2)-TMP)+CNDO(1)))/(1.+MW*(NW*(M+1.)+K2)/CL)
      TW(1)=H(1)/CL+TMP
      IF(H(1).GE.HLMP)GO TO 15
      JP=4
      GO TO 10
   15 T1=TW(1)
      K1=K2
      IF(ICV.NE.0)GO TO 16
      CALL CONVE(TOLD,TW(1),CMAX,ICV)
   16 JW1=JW-1
      IF(JW.EQ.2)GO TO 28
```

```
      DO 27 J=2,JW1
C
C  CALCULATION OF ENTHALPYS AND TEMPERATURES IN THE INTERIOR OF
C  THE ICE-WATER LAYER
C
      TOLD=TW(J)
      IW=2
      IF(J.EQ.JW1) IW=3
      IF(IGS.NE.1)GO TO 19
      CALL PHASE(IW,HO(J),HO(J+1),JPO,KO2)
      CNDO(J)=KO1*(TWO(J-1)-TWO(J))-KO2*(TWO(J)-TWO(J+1))
      KO1=KO2
   19 CALL PHASE(IW,H(J),H(J+1),JP,K2)
      GO TO(20,21,21,22),JP
C  ICE
   20 H(J)=(HO(J)+.5*MW*(K1*TW(J-1)+K2*TW(J+1)+CNDO(J)))
     1/(1.+.5*MW*(K1+K2)/CS)
      TW(J)=H(J)/CS
      IF(H(J).LE.HSMP)GO TO 25
      JP=1
C  M.P.
   21 H(J)=HO(J)+.5*MW*(K1*(TW(J-1)-MP)-K2*(MP-TW(J+1))
     1+CNDO(J))
      TW(J)=MP
      IF(H(J).GT.HSMP.AND.H(J).LT.HLMP)GO TO 25
      IF(JP.EQ.1.OR.JP.EQ.4)GO TO 25
C  LIQ. WATER
   22 H(J)=(HO(J)+.5*MW*(K1*(TW(J-1)-TMP)-K2*(TMP-TW(J+1))
     1+CNDO(J)))/(1.+.5*MW*(K1+K2)/CL)
      TW(J)=H(J)/CL+TMP
      IF(H(J).GE.HLMP)GO TO 25
      JP=4
      GO TO 20
   25 K1=K2
      IF(ICV.NE.0)GO TO 27
      CALL CONVE(TOLD,TW(J),CMAX,ICV)
   27 CONTINUE
C
C  CALCULATION OF ENTHALPY AND TEMPERATURE AT THE OUTER-AMBIENT
C  INTERFACE
C
   28 TOLD=TW(JW)
      IF(IGS.NE.1)GO TO 29
      CNDO(JW)=KO1*(TWO(JW-1)-TWO(JW))
   29 K2=-1.
```

```
      CALL PHASE(2,H(JW),H(JW),JP,K2)
      GO TO(30,31,31,32),JP
C     ICE
   30 H(JW)=(HO(JW)+MW*NA2W*(2.*TA2-TWO(JW))+MW*(K1*TW(JW-1)
     1+CNDO(JW)))/(1.+MW*(NA2W+K1)/CS)
      TW(JW)=H(JW)/CS
      IF(H(JW).LE.HSMP)GO TO 35
      JP=1
C     M.P.
   31 H(JW)=HO(JW)+MW*NA2W*(2.*TA2-MP-TWO(JW))+MW*(K1
     1*(TW(JW-1)-MP)+CNDO(JW))
      TW(JW)=MP
      IF(H(JW).GT.HSMP.AND.H(JW).LT.HLMP)GO TO 35
      IF(JP.EQ.1.OR.JP.EQ.4)GO TO 35
C     LIQ. WATER
   32 H(JW)=(HO(JW)+MW*NA2W*(2.*TA2-TMP-TWO(JW))+MW*(K1
     1*(TW(JW-1)-TMP)+CNDO(JW)))/(1.+MW*(NA2W+K1)/CL)
      TW(JW)=H(JW)/CL+TMP
      IF(H(JW).GE.HLMP)GO TO 35
      JP=4
      GO TO 30
   35 K2=1.
      IF(ICV.NE.0)RETURN
      CALL CONVE(TOLD,TW(JW),CMAX,ICV)
      RETURN
      END
C
      SUBROUTINE PHASE(IH,H1,H2,JJP,K2)
C
C     PHASE DETERMINES THE PHASE AROUND A NODE, AND SETS PHASE
C     DEPENDENT CONSTANTS
C
      IMPLICIT REAL(K-N)
      COMMON /AREA1/MP,HSMP,HLMP,HMP,CS,CL,TMP,KS,KL
      DIMENSION H(2),JP(2),K(2)
      H(1)=H1
      H(2)=H2
      DO 20 I=1,2
      IF(H(I).LE.HSMP) JP(I)=1
      IF(H(I).GT.HSMP.AND.H(I).LT.HMP) JP(I)=2
      IF(H(I).GE.HMP.AND.H(I).LT.HLMP) JP(I)=3
      IF(H(I).GE.HLMP) JP(I)=4
   20 CONTINUE
      JJP=JP(1)
      IF(K2.LT.0.) RETURN
```

```
C
C  SETTING OF PHASE DEPENDENT CONSTANTS
C
      GO TO(25,30,26),IH
   25 IF(JP(1).NE.2.AND.JP(1).NE.3)GO TO 30
      H(1)=HMP+.5*(H(1)-HSMP)
      JP(1)=3
      GO TO 30
   26 IF(JP(2).NE.2.AND.JP(2).NE.3)GO TO 30
      H(2)=HMP-.5*(HLMP-H(2))
      JP(2)=2
   30 JP1=JP(1)
      GO TO(31,31,32,33),JP1
   31 K(1)=KS
      GO TO 35
   32 X=(HLMP-H(1))/(HLMP-HSMP)
      K(1)=2.*X*KS+(1.-2.*X)*KL
      GO TO 35
   33 K(1)=KL
   35 JP2=JP(2)
      GO TO(41,42,43,43),JP2
   41 K(2)=KS
      GO TO 45
   42 Y=(H(2)-HSMP)/(HLMP-HSMP)
      K(2)=2.*Y*KL+(1.-2.*Y)*KS
      GO TO 45
   43 K(2)=KL
   45 K2=.5*(K(1)+K(2))
      RETURN
      END
/*
//GO.FT06F001  DD SYSOUT=A,OUTLIM=9900
//GO.SYSIN DD *
II= 5, P1=1, P2=1, P3=1, P4=1, P5=1, P6=1, P7=1
       P8=0, P9=1,P10=1,P11=1,P12=0,P13=0,P14=0
  JJ=       15       10        2        5        7       31
   L=     .087      .05     .004      .01     .012     0.25
   K=     66.5      .22      7.6      .22      8.7    1.416
 DIF=     1.65    .0087     .138    .0087      .15    .0492
  PI=
  HI=
  IQ=        3, C1=        , C2=    25., C3=        , A4=        , A5=
 TMO=    10.,TMF=    20.
 TIN=    -4.,TA1=    -4.,TA2=    -4., H1=        1., H2= 1000000
 ISI=        ,ISM=        ,DTMI     .1,DTMM        ,DTMF
```

```
 ISF=    250,IFRQ      5,CMAX   .005
 IWI=     50,IWM=    150, WI=   1.70, WM=  1.50, WF=  1.30
  IX=      5, JX=      7,TMAX   32.0
 CPS=  .5020, KS= 1.416,DENS   57.4, MP=   32., DH= 143.4
 CPL=   .997, KL=   .32,DENL   62.4
  JW=     31,JSH=       , LW=   .25
     ***** STANDARD DE-ICER DESIGN *****
/*
```